minerals

MDPI

Article

Geochronology, Whole-Rock Geochemistry, and Sr–Nd–Hf Isotopes of Granitoids in the Tongshanling Ore Field, South China: Insights into Cu and W Metallogenic Specificity

Yuyu Tang, Hua Kong *, Biao Liu, Qi Zong, Qianhong Wu, Hua Jiang and Fucheng Tan

Key Laboratory of Metallogenic Prediction of Nonferrous Metals and Geological Environment Monitoring, School of Geosciences and Info-Physics, Central South University, Ministry of Education, Changsha 410083, China; tangyuyu@csu.edu.cn (Y.T.); biaoliu@csu.edu.cn (B.L.); zq66666@csu.edu.cn (Q.Z.); qhwu@csu.edu.cn (Q.W.); huajiang@csu.edu.cn (H.J.); tanfucheng@csu.edu.cn (F.T.)

* Correspondence: konghua@csu.edu.cn

Abstract: The Qin-Hang Metallogenic Belt (QHMB), an important metallogenic belt in South China, hosts Cu and W–Sn polymetallic deposits. The Tongshanling ore field in the QHMB is characterized by the coexistence of Cu- and W-bearing polymetallic deposits, which are related to granodiorite and granite porphyry. This study examined whole-rock geochemistry, geochronology, and Sr–Nd–Hf isotopes to determine the genetic relationship between diverse ore-related granitoids (i.e., granodiorite and granite porphyry) and Cu–W metallogeny in the Tongshanling ore field. Zircon LA-ICP-MS U–Pb dating shows that the granodiorite and granite porphyry in the Tongshanling ore field were emplaced at 163.7 ± 0.4 Ma to 154.7 ± 0.6 Ma and 161.1 ± 0.3 Ma, respectively. Geochemically, the granodiorites are classified as oxidized I-type, while the highly evolved granite porphyry is reduced A-type. The Lu–Hf isotopic composition of the granodiorites is characterized by εHf(t) values ranging from –10.49 to –4.99 (average = –7.17), with corresponding $T_{DM}{}^{C}$ ages ranging from 1524 to 1877 Ma (average = 1682 Ma). In contrast, the granite porphyry has higher εHf(t) values (–3.60 to –1.58, average = –2.78) and younger $T_{DM}{}^{C}$ (1310–1438 Ma, average = 1387 Ma). The εNd(t) values of granodiorite are −8.06 to −7.37 and the two-stage model ages (T_{DM2}) are 1543–1598 Ma, while the granite porphyry has higher εNd(t) values (−3.0 to −3.4) and younger T_{DM2} ages (1195–1223 Ma). The results show that the granodiorite and granite porphyry were formed from partial melting of different Mesoproterozoic basement rocks under varying degrees of crust–mantle interaction. Granite porphyry underwent well-recorded fractional crystallization. Compared to the Cu-forming granodiorite, the W-forming granite porphyry has a higher differentiation index, higher crystallization temperatures of zircon (average = 708 °C versus 631 °C), and lower oxygen fugacity (median ΔFMQ = –2.21 versus –1.77).

Keywords: I-type granite; A-type granite; Cu–W mineralization; W mineralization; Qin-Hang metallogenic belt

check for updates

Citation: Tang, Y.; Kong, H.; Liu, B.; Zong, Q.; Wu, Q.; Jiang, H.; Tan, F. Geochronology, Whole-Rock Geochemistry, and Sr–Nd–Hf Isotopes of Granitoids in the Tongshanling Ore Field, South China: Insights into Cu and W Metallogenic Specificity. *Minerals* **2022**, *12*, 892. https://doi.org/10.3390/min12070892

Academic Editor: Jean-Michel Lafon

Received: 1 June 2022
Accepted: 11 July 2022
Published: 15 July 2022

1. Introduction

The Qinzhou-Hangzhou Metallogenic Belt (QHMB), located within the suture zone of the Yangtze Block and Cathaysia Block (South China), underwent multiple tectonism and magmatism in the Phanerozoic and hosts numerous Cu and W polymetallic deposits (Figure 1a,b) [1–3]. Previous studies suggested that the ore-related granitoids in the QHMB include I-type and A-type granitoids formed during the Mesozoic [4–8]. The weakly fractionated and oxidized I-type granitoids are commonly associated with 170–150 Ma Cu polymetallic mineralization [8–12]. In contrast, the highly fractionated and reduced A-type granitoids have a stronger genetic relationship with W–Sn polymetallic mineralization [8,9,11–16]. Typical examples of the I-type granitoids include the granodiorite porphyry in the Baoshan Cu polymetallic deposit [17–20] and the granodiorite in the Tongshanling Cu polymetallic deposit [8,12,21–23], while the A-type granitoids are represented by alkali-feldspar granites in the Xianghualing Sn (W) polymetallic deposit [18–20] and biotite granites in the Shizhuyuan W (Sn) polymetallic deposit [12,24–26]. In addition, A- and I-type granitoids can be present within a single deposit and are related to different mineralization types, such as granite porphyry and quartz porphyry in the Huangshaping Cu–Sn–W deposit [27–32]. Therefore, the ore-forming granites of the Cu and W deposits in the QHMB have different geochemical characteristics, such as differentiation index formation temperature, and oxygen fugacity.

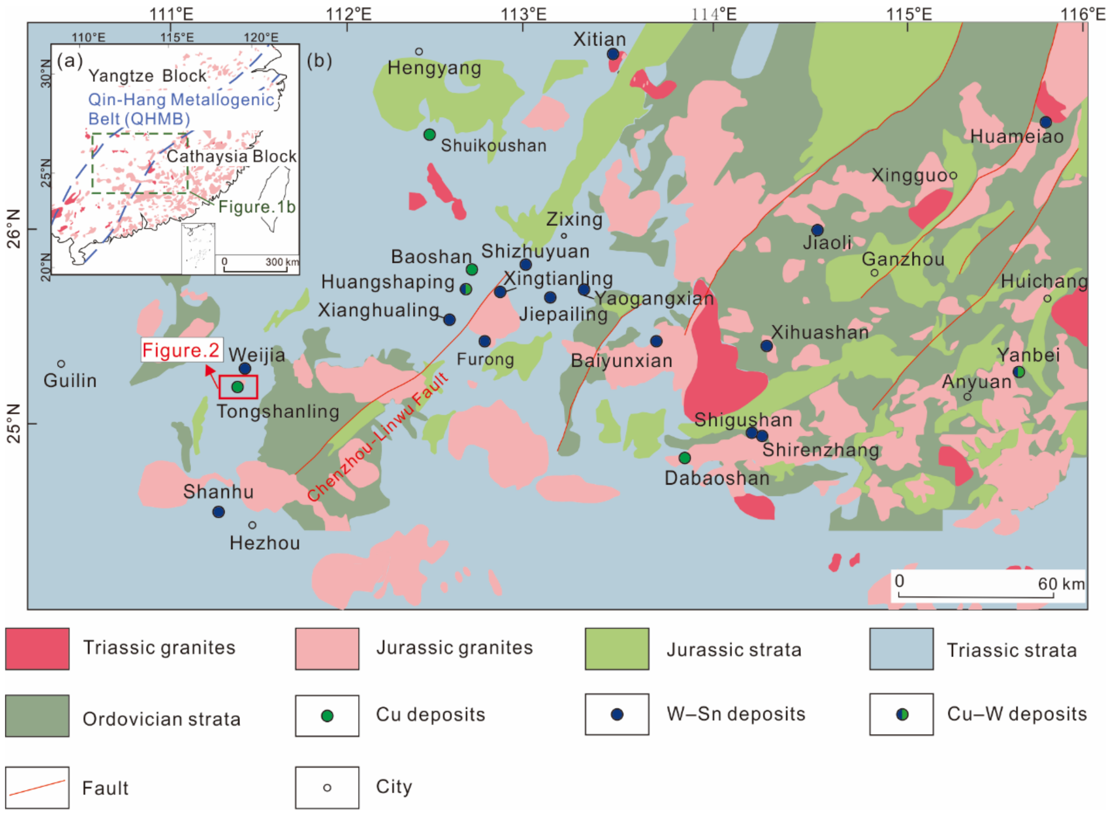

Figure 1. Distribution of (**a**) Triassic and Jurassic granitoids in South China, (**b**) the Cu and W-Sn ore deposits location of the Qin–Hang ore belt (after [3,12,20]).

However, many researchers have found W mineralization in Cu deposits [33]. This phenomenon is also present in the Tongshanling ore field, where W mineralization is found in both skarn and quartz veins [34,35]. In addition, large W ore bodies have been discovered from drill cores in the Tongshanling ore field (Figure 2). The magmatic rocks in the Tongshanling ore field mainly include granodiorite and granite porphyry. Previous work focused on the Cu mineralization age and source of ore-forming materials [8,21–23]. For example, Kong et al. (2018) [22] conducted U–Pb dating on Tongshanling granodiorites No. 1 (~166 Ma) and No. 3 (~148 Ma), which indicated that the Tongshanling granodiorites have multi-stage emplacement. Based on the S and Pb isotopic compositions of sulfides in different Cu–Pb–Zn deposits in the QHMB (e.g., Shuikoushan, Tongshanling, Baoshan, and Qibaoshan deposits), Li et al. (2019) [23] believed that Cu came from magmatic-hydrothermal solution, while Pb–Zn came from surrounding rock strata. Ding et al. (2015) [8] compared the geochemical compositions of apatite from granitoids associated with Cu–Pb–Zn (e.g., Tongshanling and Baoshan deposits) and W–Sn mineralization (e.g., Xintianling and Furong deposits) and suggested that the former were formed at high oxygen fugacity. Furthermore, the magmatic source was rich in mantle-derived materials [8–11]. W–Sn-mineralization-related granitoids were formed at low oxygen fugacity from partial melting of metasedimentary sources [36–38]. The Tongshanling ore field is a wonderful window to understand the metallogenic specificity of Cu- and W-forming granitoids and to identify the processes of W-mineralization-related granitoids, which are currently not clear.

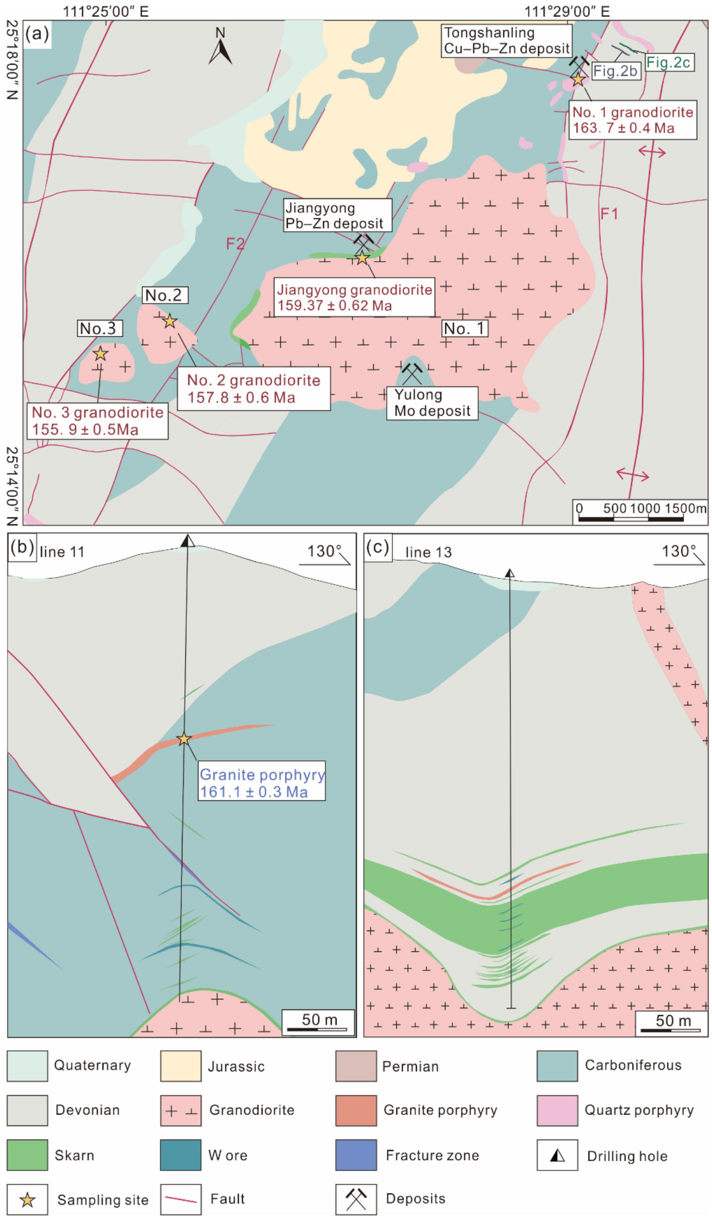

Figure 2. Geological map of (**a**) the Tongshanling area in southern Hunan Province (after [21]). Representative geological sampling location and cross–sections of (**b**) No. 11 exploration line and (**c**) No. 13 exploration line of the Tongshanling ore field.

In this contribution, we report the whole-rock geochemistry, Sr–Nd isotopes, zircon U–Pb dating, and zircon Hf isotopes of the granodiorites and granite porphyry in the Tongshanling ore field. This study aims to determine the petrogenesis of the granitoids (petrogenetic type, magma source, oxygen fugacity, temperature, and emplacement age) and address the relationship between different magmatic rocks and metallogenic processes in order to shed new light on coupled Cu–W metallogeny in the QHMB.

2. Geological Setting

2.1. Regional Geology

The QHMB is located at the suture zone of the Yangtze Block and the Cathaysia Block (Figure 1a) [1–3]. This belt, which has a NE-trending inverse S shape (Figure 1b), extends from Qinzhou in the southwest, through southeast Hunan and central Jiangxi to Hangzhou in the northeast, with a total length of ~2000 km and a width of 100–150 km [39–41]. Sedimentary strata of Preambrian, Cambrian, Ordovician, Devonian, Carboniferous, Permian, Triassic, Jurassic, and Cretaceous ages are exposed in this area. The initial enrichment or formation stage of mineralization in this belt occurred before the Paleozoic. The Triassic was a stage of further enrichment of ore-forming materials. During the Jurassic, a large-scale lithospheric extension resulted in granitic magmatism and intrusion, and the accumulation of ore-forming materials finally contributed to mineralization in the QHMB [39–42]. The mineralization is represented by Cu polymetallic deposits (e.g., Tongshanling, Dexing, and Baoshan) [8,12,17,21–23], W (Sn) polymetallic deposits (e.g., Xianghualing and Shizhuyuan) [12,18–20,24–26,43], and Cu and W (Sn) polymetallic deposits (e.g., Huangshaping) [27–32], which are porphyry-, skarn-, and hydrothermal-type deposits. The contemporaneous granitoids generally have weakly peraluminous and high-K calc-alkaline compositions, except for the high-Mg characteristics of granodiorite porphyry in Dexing [8,12,17]. In the QHMB, granitoids associated with mineralization have relatively high $\varepsilon Nd(t)$ (>–8) and low T_{DM} (<1.5 Ga), reflecting mantle–crust interaction [44].

2.2. Ore Field Geology

The Tongshanling ore field is located in the central-western QHMB and is composed of multiple granodiorites (e.g., No. 1, No. 2, and No. 3) from the east to the west (Figure 2a). Quartz porphyry occurs in the vicinity of Maozaiwan in the NE segment of Tongshanling and Monzogranite outcrops in the NE part of No. 1. The total outcrop area of the granitoids is about 13 km^2, and it intrudes into the surrounding rock in the shape of a jellyfish (Figure 2a). In addition, this study found that there are granite porphyries at depth in the Tongshanling ore field. The regional strata are mainly Devonian and Carboniferous, and the lithology is mainly limestone, argillaceous limestone, dolomitic limestone, and dolomite. Sedimentary rocks are exposed on top of upper Paleozoic and Cenozoic sediments. The north of the mining area is composed of gray, thick, siliceous concretions, mica, and argillaceous limestones. The south part consists of black, medium, silty mudstone, gray calcarenite, thin argillaceous limestone, and dark-gray micrites intercalated with dolomite, with a thickness of 350 m.

The compound folds of the ore field include the Dayuanling anticline, Beihoushan syncline, and Niuyanjing anticline, among which the Beihoushan syncline is closely related to ore bodies. The Beihoushan syncline is located between faults F2 and F1 and is composed of lower Carboniferous and Permian strata, which are the main rock formation and ore-controlling structures in the Tongshanling ore field. The Tongshanling granodiorite is intruded along the synclinal axis, and irregular polymetallic ore bodies are distributed in the contact zone between the synclinal Devonian strata and the granodiorite. The edge facies of Tongshanling granitoids contains disseminated mineralization. Fault structures are developed in which the granodiorites and orebodies are controlled by NNE trending faults in the Tongshanling ore field. There are abundant Cu–Pb–Zn orebodies around the faults [45]. The skarn-type Cu (W) polymetallic mineralization related to Jurassic granodiorite is emplaced into the upper carbonate limestone. Skarn-type Cu (W) ore bodies and quartz-vein-type W (Cu) ore bodies are controlled by the Tongshanling granodiorite contact zone. Skarn-type ore bodies are developed in the contact zone between granodiorite and Devonian strata. Quartz-vein-type bodies are distributed in granodiorite, skarn orebodies, and wall rock, which are in a tangential relationship with wall rock. In recent years, a medium-large scheelite deposit was found in the Weijia area (northeast of Tongshanling) [46,47], and large W(Mo) ore bodies have been verified at depth in the Tongshanling ore field (Figure 2b,c). The W ore body, which is stratified with an average dip of 35.5°, mainly occurs in the skarn interlayer in the Devonian wall rock in the contact zone of granite porphyry. This W ore body is only controlled by two boreholes, ZK1101 and ZK1301, and its size remains to be further determined.

The Tongshanling No. 1 granodiorite is grayish-white with medium-grained, massive, and porphyritic texture, and is composed of plagioclase (~35%), potassium feldspar (~25%), quartz (~25%), biotite (~10%), and hornblende (~5%). Plagioclase (~5 mm), potassium feldspar (~5 mm), quartz (~15 mm), biotite (~3 mm), and hornblende (~1 mm) are phenocrysts, and the same set of minerals constitutes the matrix (<0.02 mm) (Figure 3a,b). The Jiangyong granodiorite is grayish-white and is characterized by medium-fine grained, massive, and porphyritic texture, and is composed of plagioclase (~35%), potassium feldspar (~25%), quartz (~20%), biotite (~13%), and hornblende (~7%). Plagioclase (~5 mm), potassium feldspar (~5 mm), quartz (~10 mm), biotite (~3 mm), and hornblende (~1 mm) comprise the porphyry, and the same minerals from the matrix (<0.02 mm) (Figure 3c,d). The Tongshanling No. 3 granodiorite is gray with fine-grained, massive texture, and is composed of plagioclase (~35%), potassium feldspar (~25%), quartz (~18%), biotite (~15%), and hornblende (~7%). The phenocrysts in the No. 3 granodiorite are small, with grain sizes of about 3 mm and 1 mm for the felsic minerals, respectively (Figure 3e–f). Granodiorites from No. 1, Jiangyong, and No. 3 are accompanied by a small amount of sericitization and chloritization; from east to west, the particle size gradually becomes fine, and felsic mineral content increases. Quartz porphyry outcrops in the NE of the Tongshanling ore field and is intensely altered. This study collected fresh granite porphyry by drilling in the Tongshanling ore field (Figure 2b). The granite porphyry is gray-green, has massive and porphyritic texture, and contains ~70% felsic matrix and ~30% porphyritic crystals, in which there is ~10% plagioclase, ~7% K-feldspar, quartz ~5%, and ~3% biotite (Figure 3g,h).

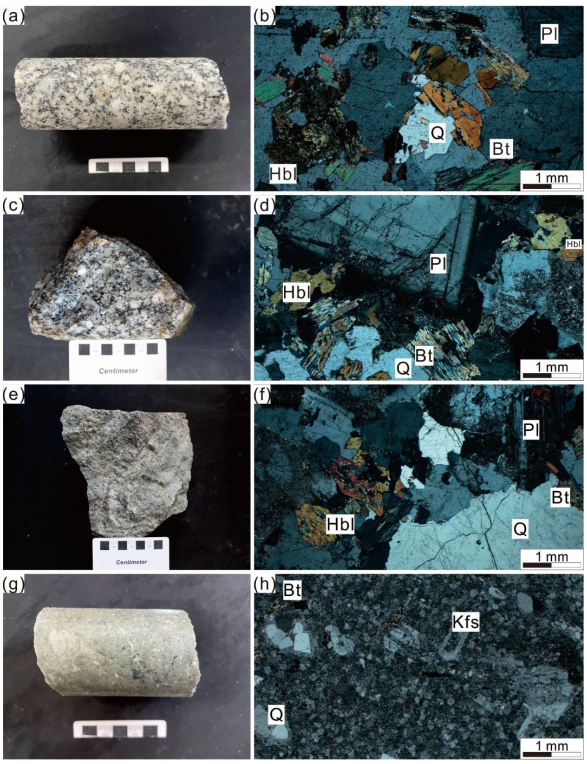

Figure 3. Photos of the Tongshanling granitoids showing variable petrography and textures: (**a**) hand specimen of No. 1 granodiorite; (**b**) photomicrograph of No. 1 granodiorite; (**c**) hand specimen of Jiangyong granodiorite; (**d**) photomicrograph of Jiangyong granodiorite; (**e**) hand specimen of No. 3 granodiorite; (**f**) photomicrograph of No. 3 granodiorite; (**g**) hand specimen of granite porphyry; (**h**) photomicrograph of granite porphyry. Bt, biotite; Hbl, hornblende; Kfs, K-feldspar; Pl, plagioclase; Q, quartz.

3. Sampling and Analytical Methods

The samples used for the analysis of the main elements in the whole rock were fresh. A total of 11 granodiorite samples were collected from Tongshanling and Jiangyong (five from the Jiangyong, three from the No. 1, and three from the No. 3). Due to the intense weathering of No. 2 granodiorite in the Tongshanling area, only zircon U–Pb dating of No. 2 granodiorite was performed. A total of three granite porphyry samples were collected from drilling, with all sample locations given in Supplementary Table S1. The granitoids collected in this study for zircon U–Pb dating include granodiorite No. 1, Jiangyong, No. 2, No. 3, and the granite porphyry.

Whole-rock major and trace element compositions were analyzed at ALS Laboratory, Guangzhou, China. The samples were crushed in a milling machine to pass 200 mesh before major element contents were measured using a PANanalytical PW2424 X-ray fluorescence (XRF) instrument made in the Netherlands, with analytical accuracy of about 1%–5%. Trace element compositions were measured using ICP–MS (Agilent 7900 made in the America with analytical accuracy of better than 5%.

Zircon cathodoluminescence (CL) images were conducted at Beijing Zhongke Kuangyan Test Technology Co. Ltd. The coarsely selected zircon grains were manually selected under a binocular microscope, and zircon grains with intact crystal shape, large particle size, and developed oscillatory belts were selected for target preparation. Before the analysis, the zircon was observed by reflected and transmitted light microscopy, the internal structure was identified by CL imaging, and the type of zircon was roughly identified to determine the analysis point. Zircon U–Pb dating and trace element analyses were conducted at the Key Laboratory of Metallogenic Prediction of Nonferrous Metals and Geological Environment Monitor of Ministry of Education, Central South University, China, on a Teledyne Photon Machines Analyte He Excimer made in the America, coupled with an Analytik Jena PlasmaQuant MS Ellite made in the America. The beam spot diameter was 35 µm, the laser pulse frequency was 5 Hz, the energy was 70 mJ, the denudation time was 60 s, and the background measurement time was 40 s. The laser ablation beam diameter and ablation depth are 32 µm and 20–40 µm, respectively. The sample standard bracket (SSB) method was performed to correct laser-induced fractionation. Zircon 91500 and GJ-1 were used as external standards for U–Pb dating. An NIST SRM610 standard silicate glass was used for external standardization for trace element analysis, and 29Si was used for internal standardization (32.8% SiO_2 in zircon). Common Pb correction was conducted by using the model of Stacey and Kramers (1975) [48]. The Isoplot R version 4.4 program was used for plotting of zircon concordant and weight mean age diagrams [49].

Experiments of in situ Hf isotope ratio analysis were conducted using a Neptune Plus MC-ICP-MS in combination with a Geolas HD excimer ArF laser ablation system that was hosted at the Wuhan Sample Solution Analytical Technology Co. Ltd., Hubei, China. All data were acquired on zircon in single spot ablation mode at a spot size of 44 µm. The ablation spots for the Hf isotope analyses were situated adjacent to the U–Pb age analysis positions on each grain. The energy density of laser ablation that was used in this study was ~7.0 J/cm^2. Each measurement consisted of 20 s of acquisition of the background signal, followed by 50 s of ablation signal acquisition. In order to ensure the reliability of the analysis data, three international zircon standards of Plešovice, 91500, and GJ-1 are analyzed simultaneously with the actual samples. Plešovice is used for external standard calibration to further optimize the analysis and test results. 91500 and GJ-1 are used as the second standard to monitor the quality of data correction.

Sr–Nd isotope composition was determined on whole-rock samples. The samples were pretreated by the acidification digestion method. After chemical separation in an ultra-clean chamber, MC-ICP-MS was used for testing at the Beijing GeoAnalysis Co. Ltd., Beijing, China. BCR-2 standard was measured together with the samples, giving a $^{87}Sr/^{86}Sr$ ratio of 0.705074 ± 0.000009 (2σ) and $^{143}Nd/^{144}Nd$ ratio of 0.512626 ± 0.000006 (2σ), in agreement with the referenced values of 0.70501 [50] and 0.51263 [51], respectively.

4. Results

4.1. Major and Trace Elements of Granitoids

Whole-rock major and trace element compositions of the four granodiorites and granite porphyry are presented in Supplementary Table S2. All the samples have low loss on ignition (LOI) values (<3.0%), suggesting a weak weathering influence.

The granodiorites have variable contents of SiO_2 (63.11%–68.48%, average = 65.95%), TiO_2 (0.38%–0.59%, average = 0.50%), FeO^T (2.86%–4.67%, average = 3.97%), MgO (1.18%–1.90%, average = 1.56%), CaO (2.85%–4.83%, average = 3.61%), and Na_2O (1.99%–3.08%, average = 2.77%) but constant contents of Al_2O_3 (14.26%–16.02%, average = 15.15%), MnO (0.08%–0.10%, average = 0.09%), K_2O (3.50%–4.51%, average = 4.00%), and P_2O_5 (0.16%–0.22%, average = 0.19%) (Figure 4a–i). The granite porphyry has higher SiO_2 (71.24%–73.78%, average = 72.80%) and K_2O (4.82%–6.51%, average = 5.42%), moderate Al_2O_3 (13.70%–14.78%, average = 14.09%) and Na_2O (0.81%–3.32%, average = 2.39%), and lower TiO_2 (0.21%–0.23%, average = 0.22%), FeO^T (2.13%–2.38%, average = 2.26%), MnO (0.06%), MgO (0.55%–1.11%, average = 0.75%), CaO (0.54%–0.71%, average = 0.62%), and P_2O_5 (0.07%–0.08%, average = 0.08%) than those of granodiorites (Figure 4a–i).

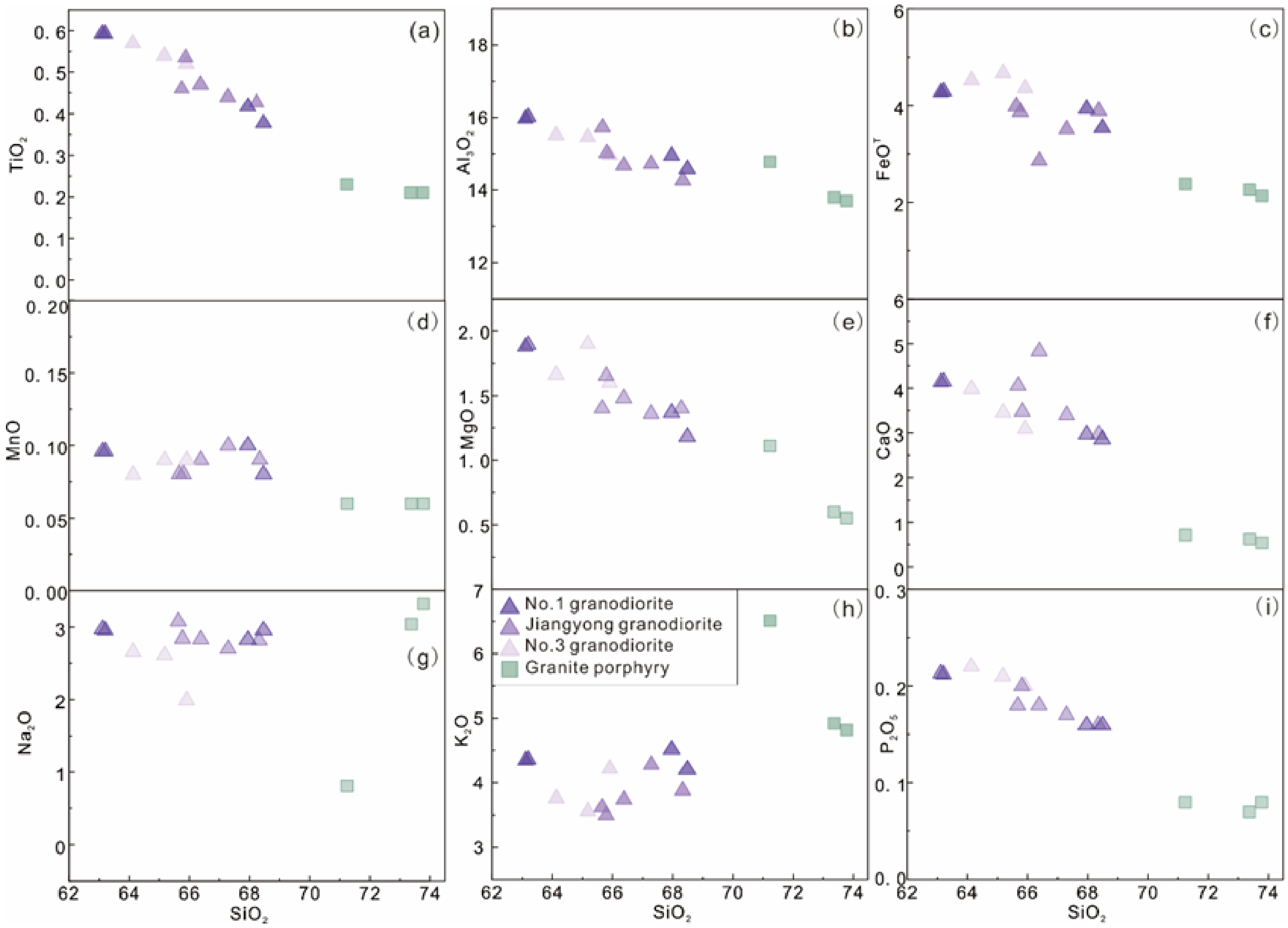

Figure 4. Harker plots for the Tongshanling granitoids: SiO_2 vs. (**a**) TiO_2; (**b**) Al_2O_3; (**c**) FeO^T; (**d**) MnO; (**e**) MgO; (**f**) CaO; (**g**) Na_2O; (**h**) K_2O; (**i**) P_2O_5.

Based on the calculation of the CIPW norm for chemical compositions, four granodiorites and granite porphyry are classified as granitoids. On the TAS diagram and R1 vs. R2 diagram (Figure 5a,b), the No. 1, Jiangyong, and No. 3 granitoids plot in the granodiorite field, whereas the granite porphyry plots in the granite field. The A/CNK values (molar Al_2O_3/(CaO + Na_2O + K_2O)) of granodiorites are characteristic of metaluminous to peraluminous composition and the granite porphyry shows peraluminous A-type granite affinity (Figure 5c). On a SiO_2 vs. K_2O diagram (Figure 5d), all rocks fall in the high-K calc-alkaline field. The Tongshanling granite porphyry (85.3–91.3) has relatively high values of differentiation index (DI), which are higher than the Jiangyong (71.7–76.5) and Tongshanling (No. 1 = 69.7–72.8; No. 3 = 70.3–81.1) granodiorites, respectively (Supplementary Table S2). The granite porphyry is high-K calc-alkaline. In contrast, the granodiorites are high-K calc-alkaline and quasi-aluminous to peraluminous, and the contents of Al_2O_3, CaO, MgO, TiO_2, and P_2O_5 are negatively correlated with SiO_2 (Figure 4a,b,e,f).

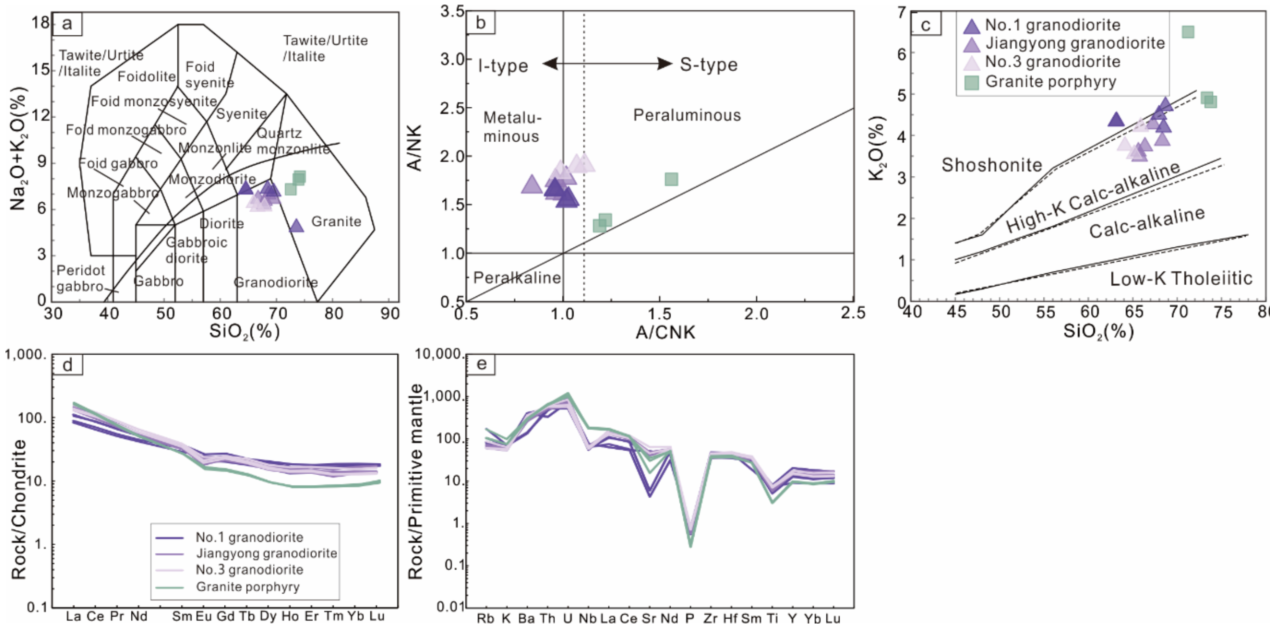

Figure 5. Geochemical classification diagrams for the Tongshanling granitoids: (**a**) TAS diagram (after [52]); (**b**) A/CNK vs. A/NK plot (where A = Al_2O_3, C = CaO, N = Na_2O, and K = K_2O in molar values, after [53]); (**c**) SiO_2 vs. K_2O plot (after [54]). Normalized trace-element patterns: (**d**) chondrite-normalized rare earth element patterns; (**e**) primitive-normalized trace-element patterns (normalization after [55]).

Trace element compositions (including rare earth elements) of all samples are listed in Supplementary Table S2. Among the granodiorites, No. 3 has the highest ΣREE values (152–173 ppm, average = 160 ppm), followed by Jiangyong granodiorite (142–157 ppm, average = 151 ppm) and No. 1 Tongshanling granodiorite (98.0–129 ppm, average = 110 ppm). The granite porphyry generally has higher ΣREE values (153–166 ppm, average = 156 ppm) than granodiorite. The Jiangyong and No. 3 granodiorites in the Tongshanling ore field are enriched in light rare earth elements (LREE) relative to HREE. The LREE/HREE ratios of the Jiangyong and No. 3 granodiorites are 7.69 to 9.88, while the No. 1 granodiorite ratios are lower, between 4.21 and 7.72. The LREE/HREE ratios of granite porphyry are higher than those of granodiorite, ranging from 14.28 to 17.11. Both lithologies show weak negative Eu anomalies (Figure 5e). The granodiorites are characterized by depletion of Nb, P, Ti, and Sr, while the granite porphyry shows more intense depletion of Sr, Ti, and P and enrichment of Nb (Figure 5f). On the chondrite-normalized REE diagrams, all samples display small Eu anomalies (Figure 5e). Granodiorites are characterized by enriched LREE and depleted HREE, whereas the granite porphyry HREE is even more depleted. On the primitive mantle-normalized trace element diagram, all samples show similar patterns characterized by enrichment in Rb, Th, U, Hf, Y, and Sm and depletion in Ba, Sr, P, Ti, and Eu (Figure 5e,f).

4.2. Zircon Morphology and U–Pb Geochronology

Zircon U–Pb dating (concordance >90%) and trace element compositions are presented in Supplementary Table S3.

Zircon grains in granodiorite samples are mainly euhedral, with lengths of 100–200 µm and aspect ratios of 1:1–3:1, and their morphologies are mainly granular and columnar. Samples have high Th/U ratios (No. 1 = 0.17–0.73, Jiangyong = 0.22–0.54, No. 2 = 0.14–0.27, and No. 3 = 0.17–0.54), which are consistent with a magmatic origin [56,57]. CL images of the zircons are shown in Figure 6. Zircon crystals in the granite porphyry are mainly euhedral, with lengths of 50–150 µm and aspect ratios of 1:1–3:1, and have high Th/U ratios (1.90–2.27), which are consistent with a magmatic origin [58]. Their morphologies are mainly granular and columnar, showing a magmatic signature of internal oscillatory zoning.

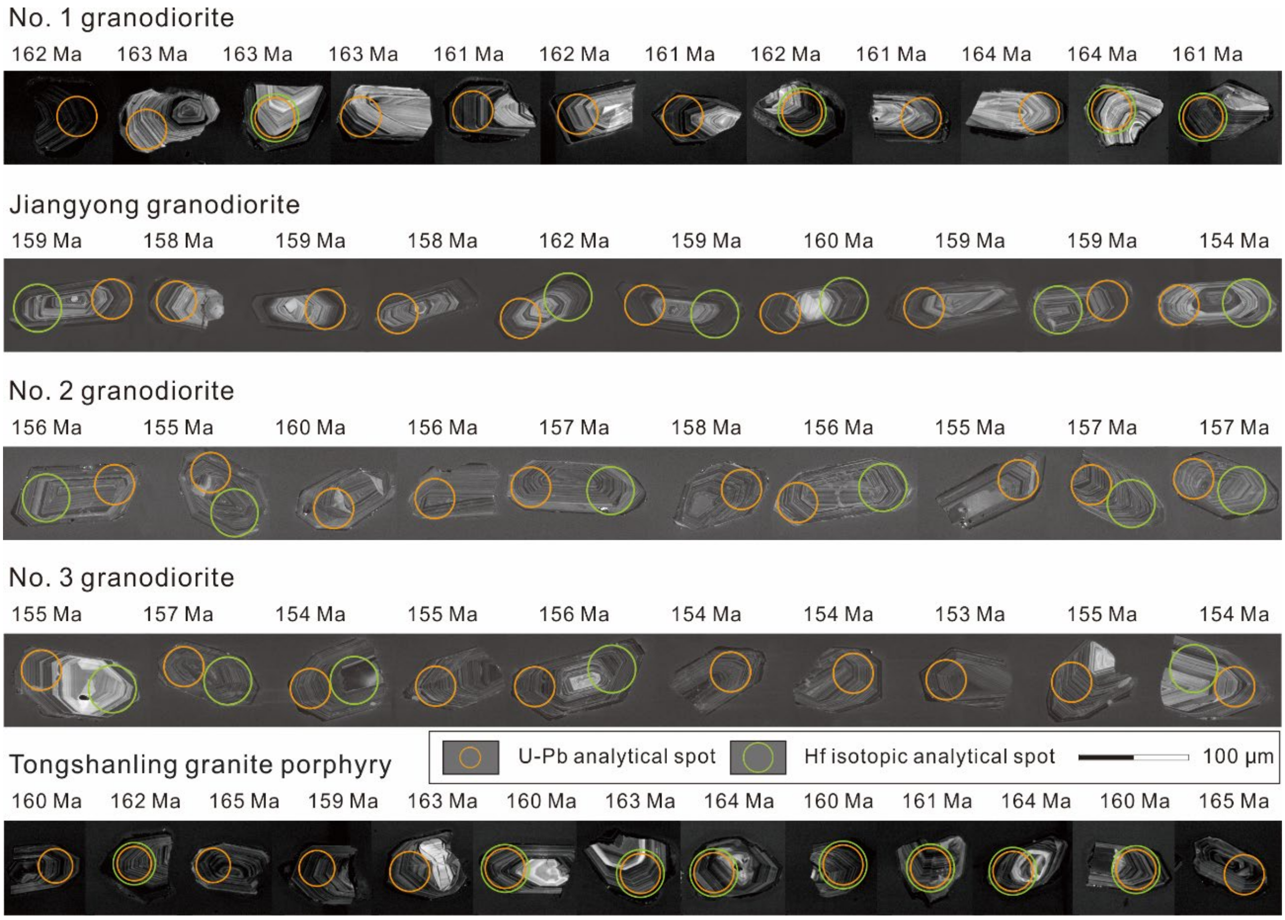

Figure 6. Cathodoluminescence (CL) images of representative zircon grains from No. 1, Jiangyong, No. 2, and No. 3 granodiorites, and granite porphyry in the Tongshanling ore field.

The LA-ICP-MS analytical results for U–Pb dating of zircons in the granitoids are shown in Supplementary Table S3. A concordia age of 163.7 ± 0.4 Ma (MSWD = 0.8, Figure 7a) was obtained for 14 zircon grains, which is the best estimate for the crystallization age of No. 1 granodiorite. An analysis of 19 zircon grains from Jiangyong granodiorite yields a $^{206}Pb/^{238}U$ concordia age of 159.4 ± 0.6 Ma (MSWD = 0.26, Figure 7b). The $^{206}Pb/^{238}U$ ages of 16 zircon grains from No. 2 granodiorite plot on or close to the concordia curve with a $^{206}Pb/^{238}U$ concordia age of 157.8 ± 0.6 Ma (MSWD = 0.2, Figure 7c). A total of 20 zircons yielded a concordia age of 154.7 ± 0.6 Ma (MSWD = 0.07, Figure 7d), indicating that the crystallization ages of the samples from No. 3 granodiorite are about 155 Ma. There are some differences in the $^{206}Pb/^{238}U$ age of granodiorite and granite porphyry. In total, 17 zircon grains yielded a $^{206}Pb/^{238}U$ concordia age of 161.1 ± 0.3 Ma (MSWD = 1.9, Figure 7e), representing the crystallization age of the granite porphyry.

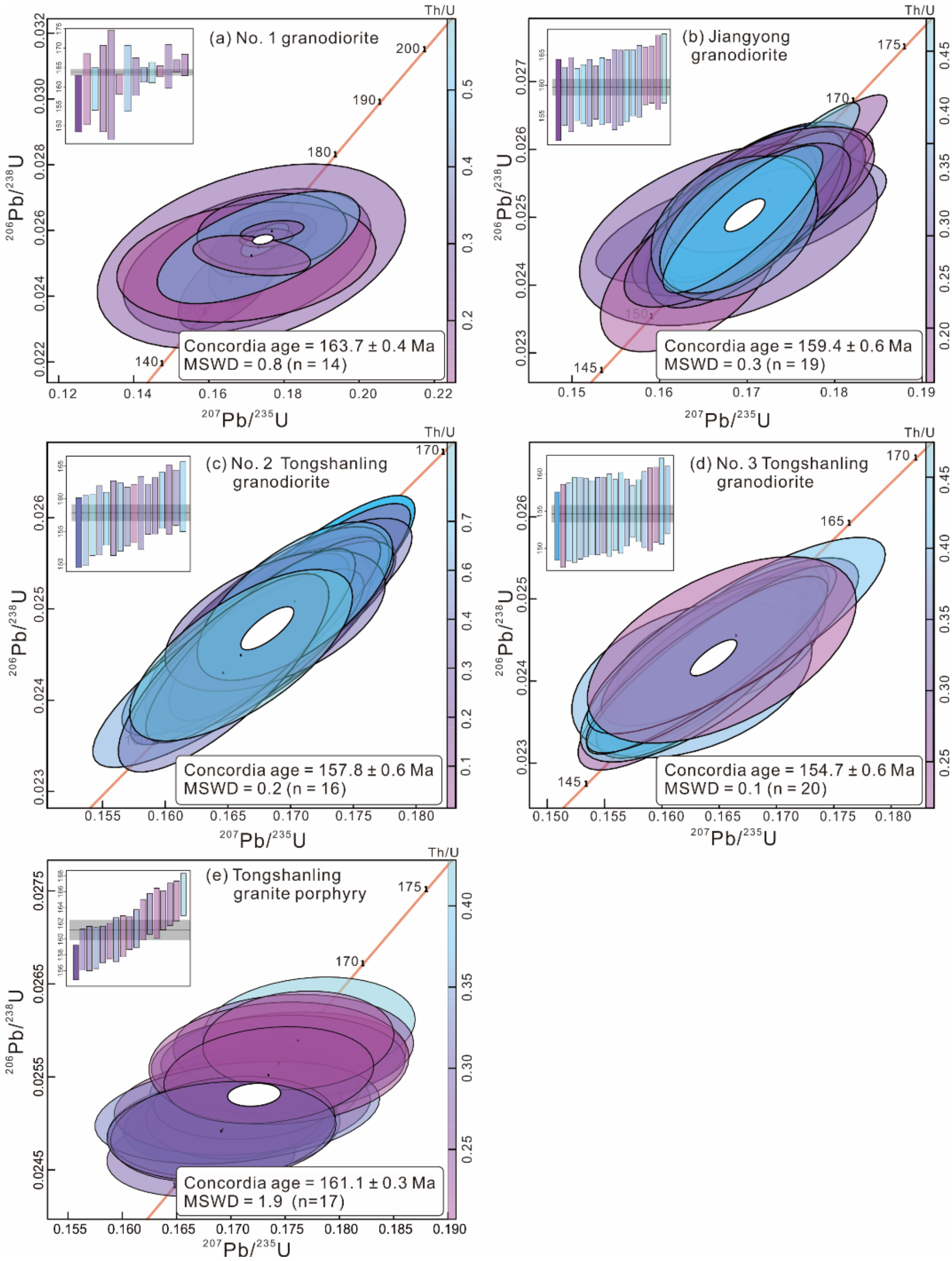

Figure 7. Concordia diagrams for UPb dating of zircons from (**a**) No. 1 granodiorite; (**b**) Jiangyong granodiorite; (**c**) No. 2 granodiorite; (**d**) No. 3 granodiorite; and (**e**) No. 1 granodiorite. Different colors of error ellipses reflect the Th/U ratios of zircons as shown on the right side of each diagram.

4.3. Zircon Lu–Hf Isotopic and Trace Element Compositions

The zircon Lu–Hf isotopic results and age model parameters for the granite in the study areas are shown in Supplementary Table S4.

The Jiangyong and No. 1, No. 2, and No. 3 granodiorites have similar zircon Hf isotopic characteristics. The Lu–Hf isotopic signature of the granodiorite zircons are characterized by variable $^{176}Yb/^{177}Hf$ (0.026182–0.110557) and $^{176}Lu/^{177}Hf$ (0.000926–0.004045). The initial $^{176}Hf/^{177}Hf$ values are 0.282378–0.282565, and εHf(t) values range from –10.49 to –3.98 (average = –7.40), with crustal model age (T_{DM}^{C}) range from 1524 to 1877 Ma (average = 1678 Ma) (Figure 8). The granite porphyry has variable $^{176}Yb/^{177}Hf$ (0.043409–0.070181) and $^{176}Lu/^{177}Hf$ (0.001229–0.002505) ratios, with initial $^{176}Hf/^{177}Hf$ and εHf(t) values ranging from 0.282577 to 0.282631 and from –3.60 to –1.58 (average = –2.78), respectively. The granite porphyry has higher εHf(t) values than the granodiorites and an average crustal model age ($T_{DM}{}^{C}$) of 1387 Ma.

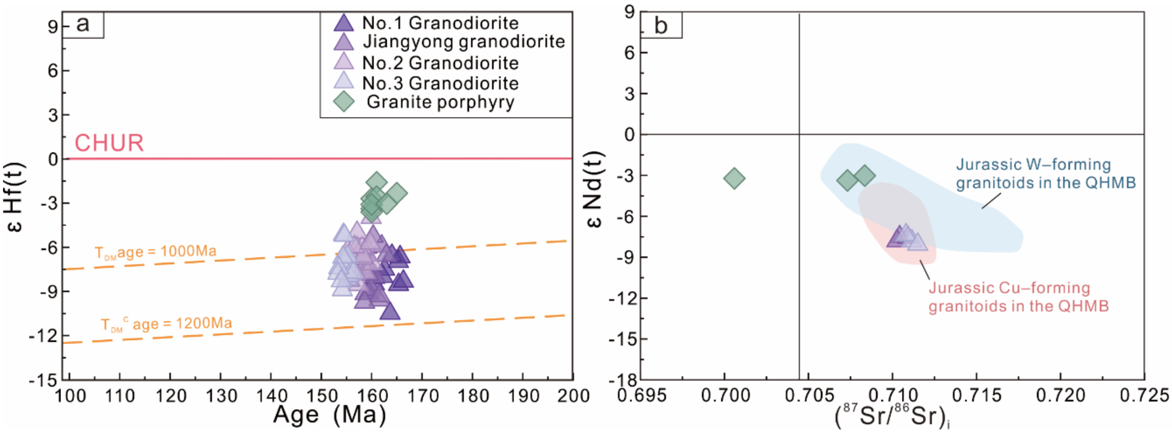

Figure 8. Plots of (**a**) zircon $^{206}Pb/^{238}U$ age vs. εHf(t) for the Tongshanling granitoids, and (**b**) $(^{87}Sr/^{86}Sr)_i$ vs. εNd(t). (Sr–Nd isotopic composition fields of the Jurassic Cu-forming and W-forming granitoids in the QHMB are after [59]).

Because the main ore-forming granitoids are No. 1 granodiorite and granite porphyry, they were used for analysis of trace elements in zircon in this study. The results of the zircon trace element and Ce^{4+}/Ce^{3+} analyses are presented in Supplementary Table S5. Zircon grains from No. 1 granodiorite have lower variable Ti (1.3–7.1 ppm) than granite porphyry (1.8–5.4 ppm). The crystallization temperature of granodiorite is 624–747 °C, which is higher than that of granite porphyry (658–753 °C). In addition, they have higher Ce^{4+}/Ce^{3+} and ΔFMQ values of 17–492 and –2.73 to –0.08 than those of the zircon grains from granite porphyry (27–266 and –2.74 to 0.31) (Figure 9).

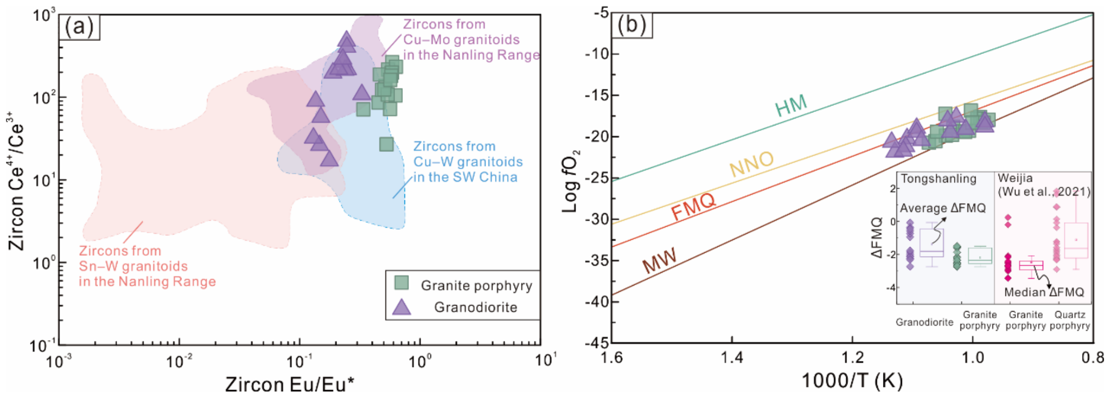

Figure 9. Plots of (**a**) zircon Eu/Eu* vs. zircon Ce^{4+}/Ce^{3+}, and (**b**) 1000/T vs. log fO_2. Zircon data of Nanling Sn–W granitoids came from [13]; zircon data of Nanling Cu–W granitoids came from [9]; zircon data for Cu–Mo granitoids in SW China came from [7]; zircon data of Weijia granitoids came from [35].

4.4. Whole-Rock Sr–Nd Isotopes

The initial ratios of $^{87}Sr/^{86}Sr$, εNd(t) values, and two-stage Nd model ages were calculated based on the zircon U–Pb ages in this study, and the isotopic data are listed in Supplementary Table S6.

The granodiorites have fairly constant initial $^{87}Sr/^{86}Sr$ values (0.710269–0.711499) and initial $^{143}Nd/^{144}Nd$ values (0.512025–0.512061). They also display relatively consistent εNd(t) (−7.37 to −8.06, average = –7.69) and two-stage Nd model ages (T_{DM2}) (1543–1598

Ma, average = 1571 Ma). Granite porphyry has relatively consistent initial $^{143}Nd/^{144}Nd$ values (0.512282–0.512302) and εNd(t) values (–3.02 to –3.37, average = –3.20), with younger T_{DM2} ages (1195–1223 Ma, average = 1209 Ma) than the granodiorites (Figure 8).

5. Discussion

5.1. Contrasting Petrogenesis of the Granodiorite and Granite Porphyry

5.1.1. Genetic Types of the Granites

I-, S-, and A-types are common criteria for classifying granitoids [60,61]. Microscopic observation shows that the Tongshanling granodiorites possess typical minerals of I-type granitoids (Figure 10, e.g., biotite and hornblende) and lack aluminum-rich minerals, such as muscovite, garnet, and cordierite [62], suggestive of an I-type origin. Geochemically, the Tongshanling granodiorites have high CaO content (>3%) and low A/CNK values (0.87–1.11) (Figure 5c). In addition, the granodiorites are characterized by notable fractionation between LREEs and HREEs, with slight negative Eu anomalies (Eu/Eu* = 0.66–0.97). On the Zr vs. 10,000 Ga/Al, Nb vs. 10,000 Ga/Al, and Al-Na-K vs. Ca vs. Fe+Mg diagrams (Figure 10a–c), the granodiorites fall within or along the boundary of I- and S-type granitoids, arguing against an A-type origin [63,64]. In addition, the negative correlation of Rb and Y further confirms that the rocks are likely of I-type rather than S-type affinity (Figure 10d) [65]. Many studies suggested that A-type granitoids are characterized by high total alkali contents ($K_2O + Na_2O > 7.0$ wt.%) and 10,000 Ga/Al ratios (mostly > 2.6) [63]. Compositionally, the Tongshanling granite porphyry has high total alkali metal contents ($K_2O + Na_2O$ = 7.32–8.14 wt.%) and high 10,000 Ga/Al ratios (>2.7). These geochemical features of A-type granitoids represent significant differences from I- and S-type granitoids [63]. Previous studies have found that there is an A-type aluminum granite belt with a high εNd(t) (>–8) and low T_{DM} (<1.5 Ga) in QHMB [44], and a large number of W–Sn deposits occur along this belt (e.g., the Xianghualing and Shizhuyuan W–Sn deposits [12,18–20,24–26]). It can be seen that the Tongshanling granite porphyry may be part of the A-type granite belt.

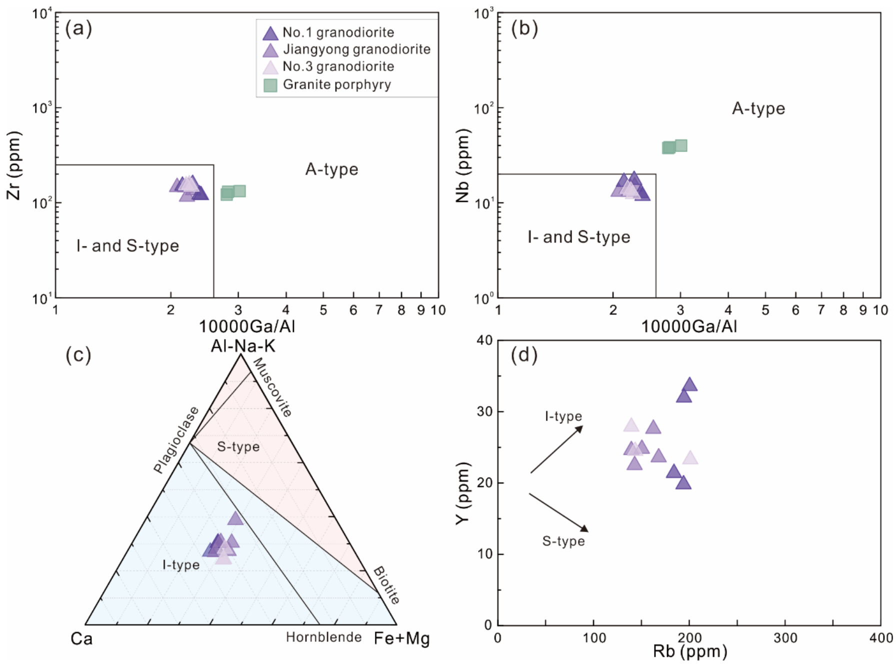

Figure 10. Petrogenetic discrimination diagrams of the studied granitoids: (**a**) 10,000 Ga/Al vs. Zr; (**b**) 10,000 Ga/Al vs. Nb; (**c**) Al–Na–K–Ca–Fe+Mg; (**d**) Rb vs. Y. (**a**,**b**) are after [63]; (**c**) is after [64]; and (**d**) is after [65].

5.1.2. Magma Generation and Evolution of the Granitoids

The petrogenesis and magma evolution of I-type melts include: (1) magmatic mixing of mantle-derived basaltic and crust-derived felsic melts [66–68]; (2) assimilation and fractional crystallization (AFC) of mantle-derived melts [69,70]; and (3) partial melting of metamorphosed mafic-intermediate rocks in the crust [71–73]. The εHf(t) values of granitoids formed by magmatic mixing usually vary from negative to positive [74], while the εHf(t) values of the Tongshanling granodiorites do not vary, indicating that the melts were not formed by magmatic mixing. Magma evolution would cause the values of La and La/Sm ratios to be inversely proportional, but Figure 11c does not show a trend of magma mixing. The lower crust is more basic and contains less Si- and Rb-rich minerals (such as quartz and feldspar) than the middle and upper crust. Therefore, AFC increases the SiO_2 and Rb/Sr of magma [75]. In addition, the SiO_2 and Rb/Sr are usually positively correlated [75]. However, the Rb/Sr ratios of the Tongshanling granodiorites are similar (mostly 0.31 to 0.80) and there is no positive correlation between SiO_2 and Rb/Sr, indicating that AFC was not extensive during the magma emplacement. The influence of fractional crystallization should also be considered. It is generally believed that only a limited quantity of granitic magmas (about 12%–25%) can be produced by fractional crystallization of mantle-derived mafic melts [76]. Therefore, the I-type granitoids formed by this process should be accompanied by large-scale contemporaneous mafic rocks around them. However, no large-scale mafic rocks were found either on the geological map or in our field survey, ruling out the possibility that the Tongshanling granodiorite was a highly fractionated product of mantle-derived melt. Together with their negative εHf(t) values, this indicates that the granodiorites were formed by partial melting of crustal basement. Additionally, due to the similar distribution coefficients, the abundances of HFSE strongly correlate in the process of partial melting but have no apparent correlation in fractional crystallization, which makes them useful for monitoring magma evolution [55]. The discrimination plots (Figure 11) indicate that the Tongshanling granite porphyry underwent fractional crystallization without significant crustal contamination during magmatic evolution. On SiO_2 vs. $(^{87}Sr/^{86}Sr)_i$, La vs. La/Sm, and Rb/Sr vs. K/Rb diagrams (Figure 11b–d), the Tongshanling granodiorites show a partial melting trend.

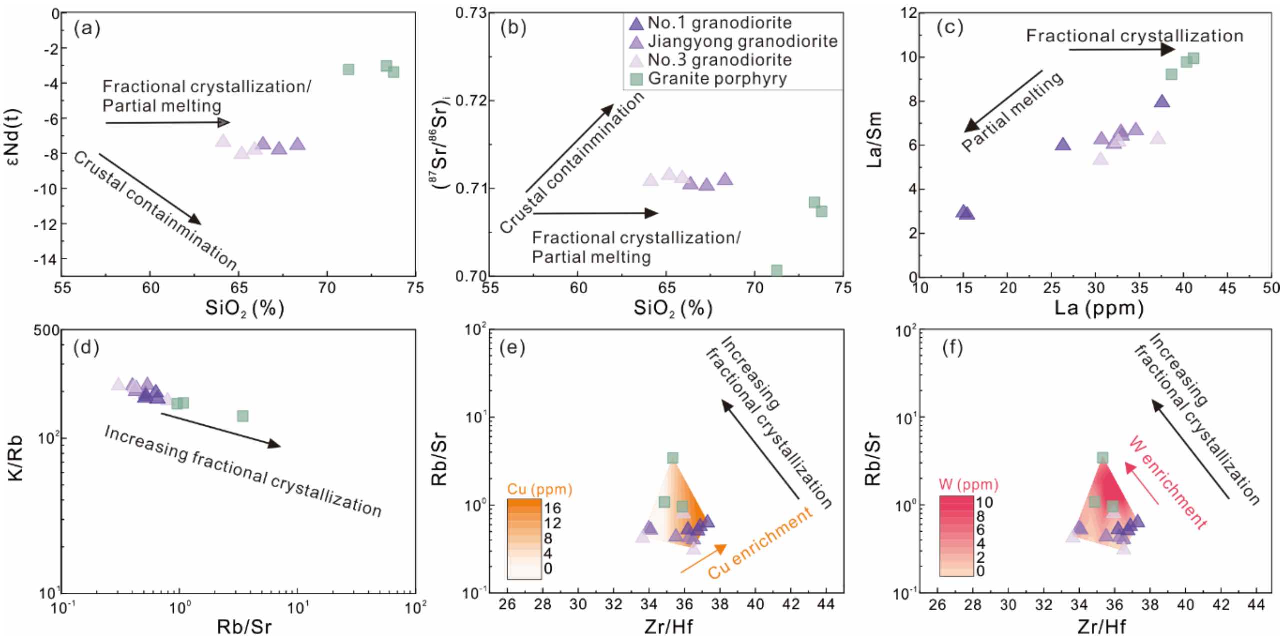

Figure 11. Plots of (**a**) SiO_2 vs. εNd(t), (**b**) SiO_2 vs. $(^{87}Sr/^{86}Sr)_i$, (**c**) La vs. La/Sm, (**d**) Rb/Sr vs. K/Rb, (**e**), Zr/Hf vs. Rb/Sr with contour map of Cu concentrations, (**f**) Zr/Hf vs. Rb/Sr with contour map of W concentrations.

5.1.3. Granite Fractionation Signatures

The high differentiation of the granite porphyry can be further documented by the high SiO_2 content (>70%), low K/Rb (<170), Zr/Hf (<36), and high DI value (>80). The contents of Sr, Ba, and Eu in the granite porphyry are depleted, indicating that the granite porphyry underwent fractional crystallization of plagioclase and K-feldspar and the presence of remnant feldspar (Figure 12a–c). The negative P anomaly indicates apatite fractionation. A positive correlation between Eu and Ba (Figure 12b) is characteristic of fractionation of plagioclase and K-feldspar. Ti, Nb, and Ta are commonly found in biotite and titaniferous minerals, such as ilmenite, rutile, and ilmenite [77], but their fractional crystallization can lead to different changes in the Ti, Nb, and Ta. Among them, the fractional crystallization of titaniferous minerals leads to a sharp drop in the Ti, Nb, and Ta in magma, while the fractional crystallization of biotite reduces the Ti and Nb but increases the Ta [78]. The FeO^T, MgO, Ti, and Nb in Tongshanling granite porphyry are low and there is no obvious Ta anomaly, indicating that biotite is present in the porphyry rather than titaniferous minerals formed by fractional crystallization.

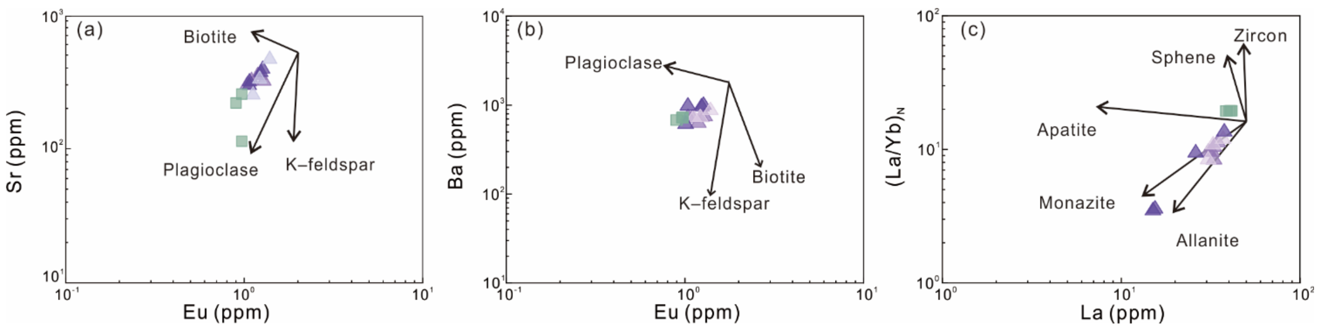

Figure 12. Plots of (**a**) Eu vs. Sr, (**b**) Eu vs. Ba, and (**c**) La vs. $(La/Yb)_N$.

The geochemical characteristics of granitoids are of great significance for determining the source of magma [64,79]. The Tongshanling granitoids are enriched LILE and depleted in Ba, Sr, P, and Ti, indicating that they are crust-derived granitoids [80]. The SiO_2 in the Tongshanling granodiorite is inversely proportional to MgO and FeO^T (Figure 4c,e), indicating that melts were generated by hornblende-rich source rocks in the middle-lower crust [81]. The basement metamorphic rock series of Cathaysia generally experienced metamorphism from greenschist facies to amphibolite facies, and some were metamorphosed from amphibolite facies to granulite facies [82,83]. The Tongshanling granodiorite is mainly distributed in the hornblende area (Figure 13a–d), indicating that it is closely related to the metamorphic basement of amphibolitic facies. The negative εNd(t) (–8.06 to –6.69) and εHf(t) (–10.49 to –2.59) and older two-stage model age of Nd (T_{DM2} = 1498–1598 Ma) and Hf ($T_{DM}{}^{C}$ = 1370–1877 Ma) indicate that Tongshanling granodiorites are the molten product of the Mesoproterozoic crust basement. Due to the high degree of differentiation of the granite porphyry, Figure 13a–d does not represent its initial magma. The granite porphyry is characterized by high SiO_2 (71.2%–73.1%) and εNd(t) (–3.02 to –3.37), and younger T_{DM2} age (1195–1223 Ma). In addition, large-scale outcrops of contemporaneous mafic rocks have not been found in the field, suggesting that the Tongshanling granite porphyry is the product of partial melting of the middle-lower crust [63,84]. The A-type granitic magma crustal source area is widely believed to have the characteristics of being anhydrous and having a high temperature. Therefore, the Mesoproterozoic granulite facies basement in South China (usually anhydrous minerals) is the potential source area for the formation of the Tongshanling A-type magma. Compared with the Tongshanling granodiorite, the higher εNd(t) values and younger T_{DM2} indicate that it is the product of partial melting of the Mesoproterozoic crustal basement.

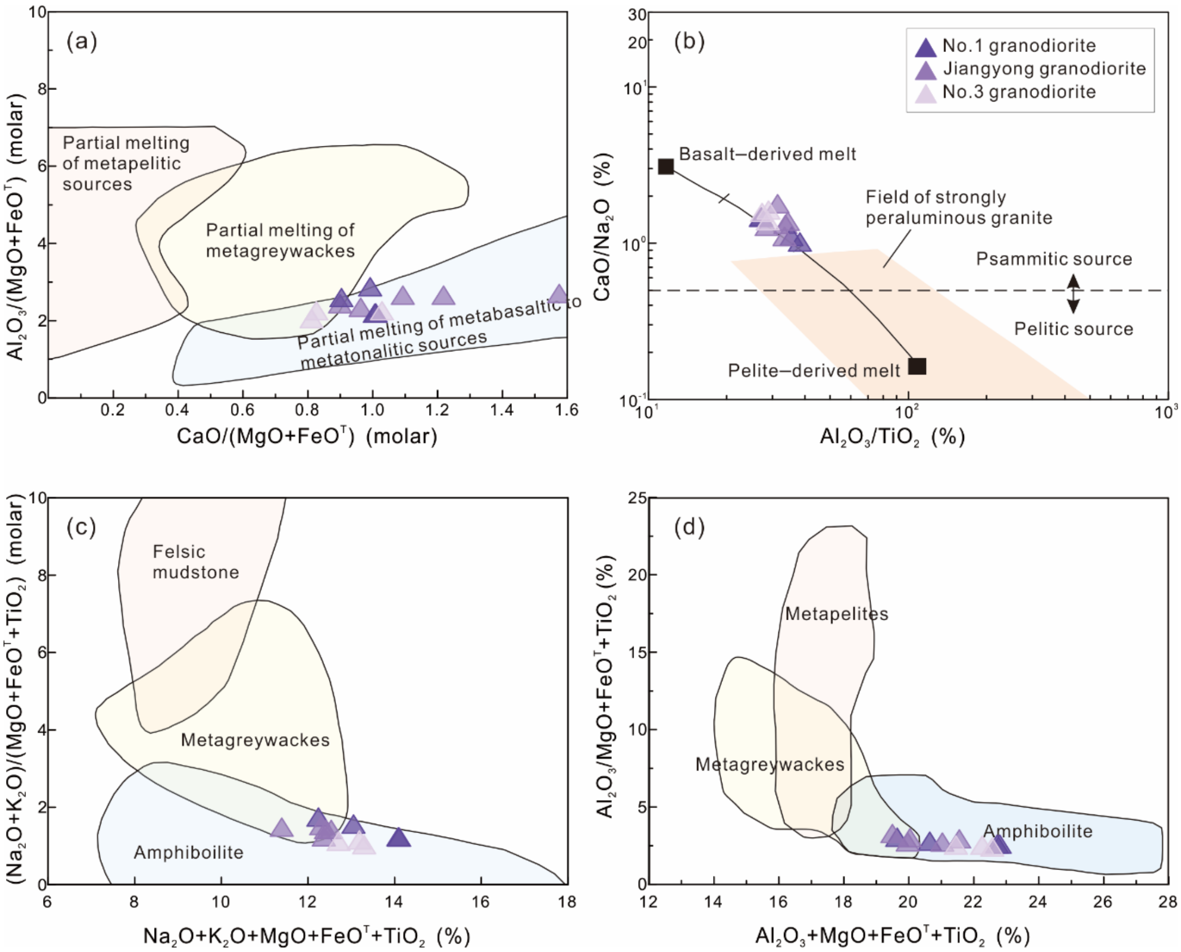

Figure 13. Plots of (**a**) molar $CaO/(MgO + FeO^T)$ vs. molar $Al_2O_3/(MgO + FeO^T)$, (**b**) Al_2O_3/TiO_2 vs. CaO/Na_2O, (**c**) $Na_2O + K_2O + MgO + FeO^T + TiO_2$ vs. molar $(Na_2O + K_2O)/(MgO + FeO^T + TiO_2)$, and (**d**) $Al_2O_3 + MgO + FeO^T + TiO_2$ vs. $Al_2O_3/(MgO + FeO^T + TiO_2)$ ((**a**) is after [85]; (**b**) is after [79]; (**c**,**d**) are after [86]).

5.2. Emplacement Age and Tectonic Implications

Jiang et al. (2009) [87] and Zhao et al. (2016) [21] conducted zircon U–Pb on Tongshanling No. 1 granodiorite at 163.6 ± 2.1 Ma and 160.7 ± 0.5 Ma, respectively. Zircon dating of the Tongshanling No. 1 granodiorite in this study gives consistent U–Pb ages of 163.7 ± 0.4 Ma (Figure 7), which are in accordance with the ages of previous studies. The metallogenic ages of the Tongshanling Cu polymetallic deposit obtained by Wu et al. (2021) [35] by cassiterites U–Pb age are 161.4 ± 3.3 Ma. The metallogenic ages are consistent with zircon U–Pb ages of the Tongshanling No. 1 granodiorite. Previous studies indicated that the No. 1 granodiorite is related to Cu–Pb–Zn polymetallic mineralization in the Tongshanling area [45,87–89], but the evolutionary relationship of No. 2 and No. 3 granodiorites to No. 1 is unclear. In this study, zircon U–Pb dating of No. 1, Jiangyong, No. 2, No. 3 granodiorites, and granite porphyry discovered in the Tongshanling area was carried out. The No. 1, Jiangyong, No. 2, and No. 3 granodiorites show a progressively younger emplacement trend from east to west (164 Ma → 159 Ma → 157 Ma → 155 Ma.). The results of the field investigation also show regularity, that is, the contents of mafic minerals, such as hornblende and biotite, in the four granodiorites decrease from east to west (Figure 3). This phenomenon observed in the field is consistent with the trend of U–Pb ages. With the evolution of magma, the mafic minerals in the magma decrease, while the felsic minerals increase. Geochemically, the Nb/Ta ratios of Jiangyong (average = 9.99), No. 1 (average = 10.39), and No. 3 (average = 10.65) granodiorites are different from those of primitive mantle (17.5, [55]) and continental crust (12.0–13.0, [90]). These differences suggest that the formation of four granodiorites took place under varying degrees of crust–mantle interaction. Furthermore, the granodiorites have sequential Lu–Hf isotopic composition, which is characterized by εHf(t) values of –7.59, –7.63, –6.47, and –7.00 for No. 1, Jiangyong, No. 2, and No. 3 granodiorites, respectively. The above evidence indicates that the degree of crust–mantle interaction gradually weakens from east to west.

At ~178 Ma, the subduction of the Paleo-Pacific plate extended to the location of southern Hunan and, from 174 Ma, slab rollback reinitiated [91]. Regional magmatism and mineralization of the Jurassic in South China are related to asthenospheric mantle upwelling induced by subduction and rollback of the Paleo-Pacific plate [3,92–100]. High-K calc-alkaline I-type granitoids are mainly formed in two tectonic settings: (1) similar to the Andean epicontinental arc, the subducting plate dehydrates, which initiates fluid metasomatism of the mantle wedge and the formation of parent magma; (2) in post-collisional environments similar to the Caledonian orogenic belt, the parent magma originates from crustal thickening during the collision, followed by post-collision decompression [101]. In the discriminant diagram of the tectonic setting (Figure 14a–c), the Tongshanling granodiorite falls within the post-collision field. The slab rollback triggered partial melting of mantle wedge and the formation of basaltic magmas [91]. The basaltic magmas can provide the heat necessary to partially melt the lower crust to produce late Jurassic I-type granitoids [102]. At the same time, due to lithospheric extension and thinning, the underplating of basaltic magmas caused partial melting of lower-crustal rocks and formed A-type granites in the Late Jurassic (163–153 Ma) [87,91,102]. The geochemical signatures of all granitoids in this study fall within the range of a post-collisional environment (Figure 14a–c), in good agreement with an extensional setting. Therefore, the Tongshanling granitoids may record magmatic activity in the context of extension caused by the subduction of the Paleo-Pacific Plate.

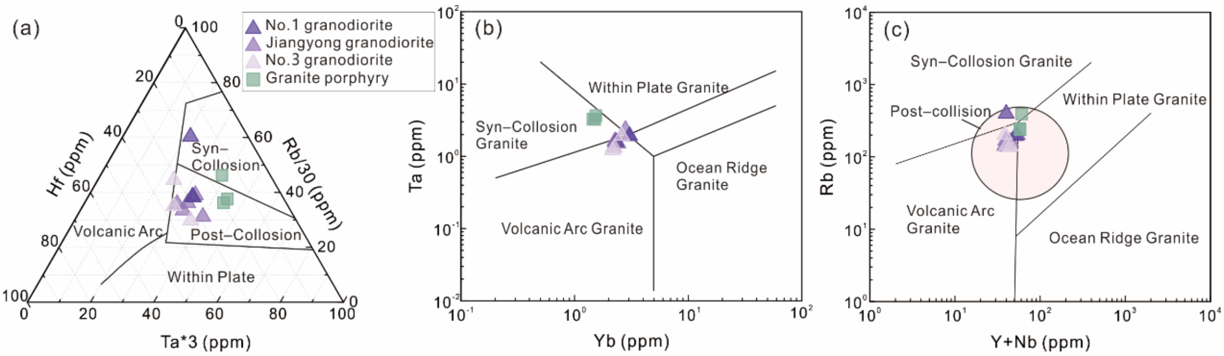

Figure 14. Discrimination diagrams for tectonic settings of formation of granitoids: (**a**) Ta*3–Rb/30–Hf ternary plot (after [103]). (**b**) Y vs. Ta and (**c**) Y + Nb vs. Rb (after [104]).

5.3. Metallogenic Specificity and Ore Genetic Model

Studies have shown that the degree of evolution of magma is an important index for studying the mineralization specificity of granitoids [105,106]. In general, Cu-rich polymetallic mineralization is associated with less evolved granitic magmatism, and W-rich polymetallic mineralization is associated with highly evolved granitic magmatism [9,105–107]. Geochemical characteristics show that the granite porphyry is alkali-rich and calcium-poor, and the differentiation index (DI = 85.3–91.2) is higher than the granodiorite (DI = 70.1–81.1), showing the characteristics of high differentiation. The ratio of Rb/Sr and K/Rb is usually used to measure the degree of magma crystal differentiation [106]. The high Rb/Sr (0.96–3.44) and low K/Rb (138–168) values of granite porphyry indicate that more intense fractional crystallization occurred during the magmatic evolution, which is accompanied by high W contents (Figure 11f). At the same time, the Th/U value of zircon in the granitoids can reflect the degree of differentiation. The Th/U value of zircon decreases with progressive crystallization and differentiation of magma [108]. The Th/U values of zircons in the two types of granitoids in the ore field indicate that the granite porphyry (0.21–0.41) in the mining area underwent more intense fractional crystallization than the granodiorite (0.15–0.52). The granodiorite is less fractionated, with high Cu contents and low Sn contents (Figure 11e,f). In summary, granite porphyry is more differentiated than the granodiorite, indicating that the W mineralization potential of the granite porphyry is higher than that of granodiorite.

Zircon has high U and Th contents, low ordinary Pb content, and high Pb diffusion sealing temperature (~900 °C), making zircon an ideal mineral to determine the crystallization age of magmatic rocks [109,110]. Zircon crystallizes in the early stage of magma cooling, and its crystallization temperature is higher than most other magmatic minerals, close to the temperature of magmatic emplacement. Many studies show that zirconium saturation temperature calculated from whole-rock Zr content can effectively represent the crystallization temperature of granitic magma. Based on the formula given by Watson and Harrison (1983) [111], we used the chemical composition of zircons from the ore-forming No. 1 granodiorite and granite porphyry to calculate their crystallization temperatures. The crystallization temperatures of zircon in granodiorite are 602–666 °C (average = 631 °C), while those in granite porphyry are 657–752 °C (average = 708 °C). The crystallization temperature of hydrothermal zircon (<500 °C) is much lower than magmatic zircons, so the crystallization temperatures of the zircons obtained in this study indicate that they are typical magmatic zircons.

Redox states also play a crucial role in the migration of metals from magmatic sources to melts [112]. Many granite porphyry and quartz porphyry veins have been identified in the Weijia area. The results show that skarn-type Cu polymetallic ore is closely related to oxidized granitic magma, while W(Sn) mineralization is mostly related to reduced granitic magma [36–38]. It is generally believed that the granite porphyry is related to the W polymetallic mineralization in Weijia [21]. The ΔFMQ of Weijia W-forming granite porphyry (median = –2.66, [35]) is lower than that of nonmineralized quartz porphyry (median = –1.65, [35]), while the Tongshanling granite porphyry (median = –2.21) is similar to Weijia W-forming granite porphyry (Figure 9b). The ΔFMQ in ore-forming No. 1 granodiorite (–2.73 to –0.08, median = –1.77) is higher than the Tongshanling granite porphyry, indicating that the granodiorite is related to Cu mineralization, whereas the granite porphyry plays an important role in the late W mineralization. Ce^{4+}/Ce^{3+} in zircon is also used to indicate the redox state of magma [112]. The I-type granodiorite has higher Ce^{4+}/Ce^{3+} (average = 182.9) than the A-type granite porphyry Ce^{4+}/Ce^{3+} (average = 146.7). In recent years, a growing body of research has found that the W-polymetallic mineralization in the Nanling area is related to the A-type granites with high differentiation and low oxygen fugacity (reduction), while the Cu-polymetallic mineralization is related to the I-type granites with weak differentiation and high oxygen fugacity (oxidation) [8–11,15]. Therefore, the granodiorite is associated with Cu mineralization, while the granite porphyry is associated with W mineralization in the Tongshanling ore field.

The following model explains the genesis and relationship of different types of granitoids in Tongshanling ore field. The Tongshanling granodiorite and granite porphyry were formed in a post-collision extensional environment (Figure 14a–c), which is consistent with lithospheric extension in the QHMB during the Mesozoic. The extension of the Middle Jurassic lithosphere resulted from the upwelling of the asthenospheric mantle, leading to heating and partial melting of the amphibolite-facies crust to form I-type granodioritic magma (~163 Ma). The high oxidation state of the magma prevented the precipitation of Cu-bearing phases. The environment of the magmatic–hydrothermal systems changed when the magma rose and reacted with the sedimentary country rock, which facilitated the precipitation of Cu–Pb–Zn ore bodies. With further extension of the lithosphere, the deep magma chamber kept pumping out magma, leading to the formation of the No. 2 and 3 granodiorites (156–160 Ma) in the late stage. After ~2 Ma, accompanying asthenosphere upwelling, crust–mantle interaction is further intensified. The magmatic source region underwent more partial melting, forming an A-type granite porphyry (~161 Ma). The reduced magma was conducive to the transport of W–Mo elements from the magmatic source region to the shallow crust for mineral deposition. The ore bodies may have been formed when hydrothermal fluid exsolved from the late granite porphyry magma and passed through the granitoids (such as granodiorite and skarn). This model is consistent with the geological phenomena observed in the Tongshanling ore field, in particular, that the quartz-vein-type ore bodies cut through the early granodiorite and skarn-type ore bodies (Figure 15).

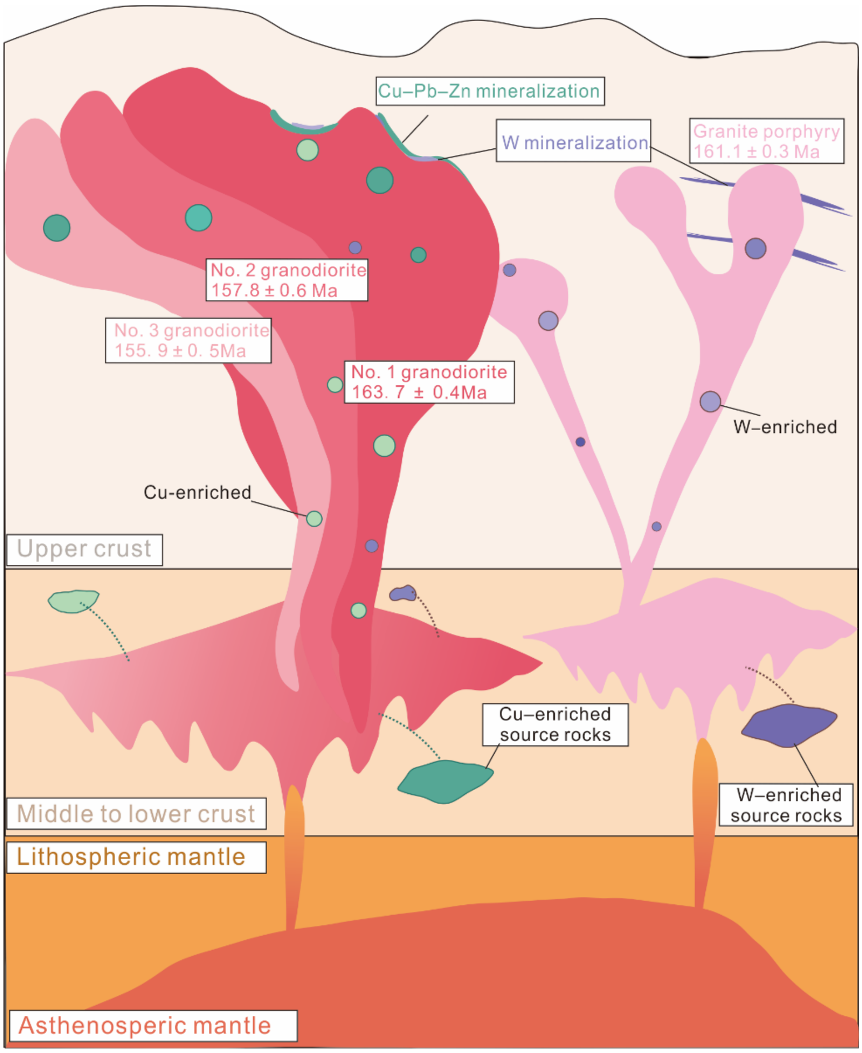

Figure 15. Schematic demonstrating multiple metallogenesis in the Tongshanling ore field: at ~163 Ma, amphibolite facies metamorphic basement partially melted to form I-type granodiorite magma, which reacted with carbonatite to form skarn Cu–Pb–Zn ore bodies. As the extension continued, magma was continuously pumped out of the cold storage, and No. 2 and No. 3 granodiorites (156~160 Ma) were formed in the late stage. Due to the magmatic activity at ~163 Ma, magmatic chambers were activated in a cold storage near the source area of granodiorite. After ~2 Ma, greater partial melting of the magmatic source region resulted in formation of granite porphyry (~161 Ma), and W ore bodies were formed when the exsolved hydrothermal fluid flowed through the felsic rock mass (such as granodiorite and skarn).

Similar to the Tongshanling ore field, Cu–Pb–Zn and W deposits are also present in the QHMB. For instance, in the Baoshan deposit, the granodiorite porphyry that is related to the Cu-forming ore body has a similar genesis as the I-type granodiorite in Tongshanling [17–20]. In the Huangshaping deposits and Xitian ore field, the A-type granite belongs to the same type as the Tongshanling granite porphyry that is related to the W-forming ore body [27–32,113]. These examples show that Cu- and W-dominated mineralization is related to the emplacement of different I-type and A-type granites in the extensional setting triggered by asthenosphere mantle upwelling [114]. These patterns of metallogenic specificity are in great accordance with characteristics of the Tongshanling ore field, which hosts skarn-type Cu ores and quartz-vein-type W ores that are related to granodiorite and granite porphyry, respectively.

6. Conclusions

(1) The Tongshanling granodiorite is I-type and was produced by partial melting of the Mesoproterozoic crustal basement. The granite porphyry has an A-type affinity, was derived from partial melting of the Mesoproterozoic basement, and underwent fractional crystallization of plagioclase and K-feldspar during its formation.
(2) The No. 1, Jiangyong, No. 2, and No. 3 granodiorites were emplaced at 163.7 ± 0.4 Ma, 159.37 ± 0.6 Ma, 157.8 ± 0.6 Ma, and 154.7 ± 0.6 Ma, respectively. The granite porphyry was emplaced at 161.1 ± 0.3 Ma. All granitoids are classified as post-collision, in good agreement with an extensional setting.
(3) The granodiorite has a low differentiation index and formation temperature, and high oxygen fugacity, which are related to Cu mineralization in the Tongshanling ore field. The granite porphyry has a high differentiation index, and formation temperature, significant crust–mantle interaction, and low oxygen fugacity, which are related to W mineralization granite porphyry in the Tongshanling ore field.

Supplementary Materials: The following supporting information can be downloaded at: https://www.mdpi.com/article/10.3390/min12070892/s1, Table S1: Sample information in the Tongshanling ore field, Table S2: The whole-rock major and trace elements compositions of Tongshanling granitoids, Table S3: Zircon LA-ICP-MS U–Pb isotopic compositions of Tongshanling granitoids, Table S4: Zircon Lu–Hf isotopic compositions for the Tongshanling granitoids, Table S5: Zircon trace elements compositions of Tongshanling granitoids, Table S6: The whole rock Sr–Nd isotopic compositions of Tongshanling granitoids.

Author Contributions: Conceptualization, Y.T. and H.K.; Data curation, Y.T. and B.L.; Formal analysis, Y.T. and H.J.; Funding acquisition, H.K. and Q.W.; Investigation, Y.T. and B.L.; Methodology, Y.T. and H.K.; Project administration, H.K.; Resources, Q.Z. and F.T.; Supervision, H.K.; Validation, Y.T. and B.L.; Visualization, Y.T.; Writing—original draft, Y.T.; Writing—review and editing, Y.T. and H.K. All authors have read and agreed to the published version of the manuscript.

Funding: This study was financially supported by the National Key Research and Development Plan (Grant No. 2018YFC0603901 and 2018YFC0603902).

Data Availability Statement: Data are contained within the supplementary materials.

Acknowledgments: We greatly appreciate Jinghua Wu for his constructive suggestions and comments to improve this work. We also thank Jeffrey Dick and Dapeng Zhu for their suggestion to this work. We appreciate editors and reviewers for their thoughtful and constructive reviews on the manuscript.

Conflicts of Interest: The authors declare no conflict of interest.

References

1. Faure, M.; Ishida, K. The Mid-Upper Jurassic Olistostrome of the West Philippines: A Distinctive Key-Marker for the North Palawan Block. *J. Southeast Asian Earth Sci.* **1990**, *4*, 61–67. [CrossRef]
2. Maruyama, S.; Isozaki, Y.; Kimura, G.; Terabayashi, M. Paleogeographic Maps of the Japanese Islands: Plate Tectonic Synthesis from 750 Ma to the Present. *Isl. Arc* **1997**, *6*, 121–142. [CrossRef]
3. Zhou, X.; Sun, T.; Shen, W.; Shu, L.; Niu, Y. Petrogenesis of Mesozoic Granitoids and Volcanic Rocks in South China: A Response to Tectonic Evolution. *Episodes* **2006**, *29*, 26–33. [CrossRef]
4. Hu, R.-Z.; Zhou, M.-F. Multiple Mesozoic Mineralization Events in South China—an Introduction to the Thematic Issue. *Miner. Depos.* **2012**, *47*, 579–588. [CrossRef]
5. Zhou, Y.; Zeng, C.; Li, H.; An, Y.; Liang, J.; Lü, W.; Yang, Z.; He, J.; Shen, W. Geological Evolution and Ore-Prospecting Targets in Southern Segment of Qinzhou Bay-Hangzhou Bay Juncture Orogenic Belt, Southern China. *Geol. Bull. China* **2012**, *31*, 486–491.

6. Guo, C.L.; Xu, Y.M.; Lou, F.S.; Zheng, J.H. A Comparative Study of the Middle Jurassic Granodiorite Related to Cu and the Late Jurassic Granites Related to Sn in the Qin-Hang Metallogenic Belt and a Tentative Discussion on Their Tectonic Dynamic Setting. *Acta Petrol. Mineral.* **2013**, *32*, 463–484.
7. Zhong, L.; Li, J.; Peng, T.; Xia, B.; Liu, L. Zircon U–Pb Geochronology and Sr–Nd–Hf Isotopic Compositions of the Yuanzhuding Granitoid Porphyry within the Shi-Hang Zone, South China: Petrogenesis and Implications for Cu–Mo Mineralization. *Lithos* **2013**, *177*, 402–415. [CrossRef]
8. Ding, T.; Ma, D.; Lu, J.; Zhang, R. Apatite in Granitoids Related to Polymetallic Mineral Deposits in Southeastern Hunan Province, Shi–Hang Zone, China: Implications for Petrogenesis and Metallogenesis. *Ore Geol. Rev.* **2015**, *69*, 104–117. [CrossRef]
9. Li, X.; Chi, G.; Zhou, Y.; Deng, T.; Zhang, J. Oxygen Fugacity of Yanshanian Granites in South China and Implications for Metallogeny. *Ore Geol. Rev.* **2017**, *88*, 690–701. [CrossRef]
10. Zhang, C.; Sun, W.; Wang, J.; Zhang, L.; Sun, S.; Wu, K. Oxygen Fugacity and Porphyry Mineralization: A Zircon Perspective of Dexing Porphyry Cu Deposit, China. *Geochim. Cosmochim. Acta* **2017**, *206*, 343–363. [CrossRef]
11. Sun, W.; Huang, R.; Li, H.; Hu, Y.; Zhang, C.; Sun, S.; Zhang, L.; Ding, X.; Li, C.; Zartman, R.E.; et al. Porphyry Deposits and Oxidized Magmas. *Ore Geol. Rev.* **2015**, *65*, 97–131. [CrossRef]
12. Mao, J.; Cheng, Y.; Chen, M.; Franco, P. Major Types and Time–Space Distribution of Mesozoic Ore Deposits in South China and Their Geodynamic Settings. *Miner. Depos.* **2013**, *48*, 267–294.
13. Shu, X.J.; Wang, X.L.; Sun, T.; Xu, X.; Dai, M.N. Trace Elements, U–Pb Ages and Hf Isotopes of Zircons from Mesozoic Granites in the Western Nanling Range, South China: Implications for Petrogenesis and W–Sn Mineralization. *Lithos* **2011**, *127*, 468–482. [CrossRef]
14. Zhou, M.F.; Gao, J.; Zhao, Z.; Zhao, W.W. Introduction to the Special Issue of Mesozoic W-Sn Deposits in South China. *Ore Geol. Rev.* **2018**, *101*, 432–436. [CrossRef]
15. Schmidt, C.; Gottschalk, M.; Zhang, R.; Lu, J. Oxygen Fugacity during Tin Ore Deposition from Primary Fluid Inclusions in Cassiterite. *Ore Geol. Rev.* **2021**, *139*, 104451. [CrossRef]
16. Ren, T.; Li, H. Research Progress of Granite-Related Tin Mineralization. *Zhongnan Daxue Xuebao Ziran Kexue Ban J. Cent. South Univ. Sci. Technol.* **2022**, *53*, 514–534. [CrossRef]
17. Lu, Y.; Ma, L.; Qu, W.; Mei, Y.; Chen, X. U-Pb and Re-Os Isotope Geochronology of Baoshan Cu-Mo Polymetallic Ore Deposit in Hunan Province. *Acta Petrol. Sin.* **2006**, *22*, 2483–2492.
18. Yuan, S.D.; Peng, J.T.; Li, X.Q.; Peng, Q.L.; Fu, Y.Z.; Shen, N.P.; Zhang, D.L. Carbon, Oxygen and Strontium Isotope Geochemistry of Calcites from the Xianghualing Tin-Polymetallic Deposit, Hunan Province. *Acta Geol. Sin.* **2008**, *82*, 1522–1530.
19. Yuan, S.; Peng, J.; Hu, R.; Li, H.; Shen, N.; Zhang, D. A Precise U–Pb Age on Cassiterite from the Xianghualing Tin-Polymetallic Deposit (Hunan, South China). *Miner. Depos.* **2008**, *43*, 375–382. [CrossRef]
20. Yuan, S.; Peng, J.; Shen, N.; HU, R.; DAI, T. 40Ar-39 Ar Isotopic Dating of the Xianghualing Sn-polymetallic Orefield in Southern Hunan, China and Its Geological Implications. *Acta Geol. Sin. Ed.* **2007**, *81*, 278–286.
21. Zhao, P.; Yuan, S.; Mao, J.; Santosh, M.; Li, C.; Hou, K. Geochronological and Petrogeochemical Constraints on the Skarn Deposits in Tongshanling Ore District, Southern Hunan Province: Implications for Jurassic Cu and W Metallogenic Events in South China. *Ore Geol. Rev.* **2016**, *78*, 120–137. [CrossRef]
22. Kong, H.; Li, H.; Wu, Q.H.; Xi, X.S.; Dick, J.M.; Gabo-Ratio, J.A.S. Co-Development of Jurassic I-Type and A-Type Granites in Southern Hunan, South China: Dual Control by Plate Subduction and Intraplate Mantle Upwelling. *Geochemistry* **2018**, *78*, 500–520. [CrossRef]
23. Li, H.; Kong, H.; Zhou, Z.K.; Wu, Q.H.; Xi, X.S.; Gabo-Ratio, J.A.S. Ore-Forming Material Sources of the Jurassic Cu–Pb–Zn Mineralization in the Qin–Hang Ore Belt, South China: Constraints from S–Pb Isotopes. *Geochemistry* **2019**, *79*, 280–306. [CrossRef]
24. Mao, J.; Li, H. Evolution of the Qianlishan Granite Stock and Its Relation to the Shizhuyuan Polymetallic Tungsten Deposit. *Int. Geol. Rev.* **1995**, *37*, 63–80.
25. Mao, J.; Li, H.; Hidehiko, S.; Louis, R.; Bernard, G. Geology and Metallogeny of the Shizhuyuan Skarn-Greisen Deposit, Hunan Province, China. *Int. Geol. Rev.* **1996**, *38*, 1020–1039.
26. Lu, H.-Z.; Liu, Y.; Wang, C.; Xu, Y.; Li, H. Mineralization and Fluid Inclusion Study of the Shizhuyuan W-Sn-Bi-Mo-F Skarn Deposit, Hunan Province, China. *Econ. Geol.* **2003**, *98*, 955–974. [CrossRef]
27. Yuan, Y.; Yuan, S.; Chen, C.; Huo, R. Zircon U-Pb Ages and Hf Isotopes of the Granitoids in the Huangshaping Mining Area and Their Geological Significance. *Acta Petrol. Sin.* **2014**, *30*, 64–78.
28. Li, H.; Watanabe, K.; Yonezu, K. Zircon Morphology, Geochronology and Trace Element Geochemistry of the Granites from the Huangshaping Polymetallic Deposit, South China: Implications for the Magmatic Evolution and Mineralization Processes. *Ore Geol. Rev.* **2014**, *60*, 14–35. [CrossRef]
29. Li, X.; Huang, C.; Wang, C.; Wang, L. Genesis of the Huangshaping W–Mo–Cu–Pb–Zn Polymetallic Deposit in Southeastern Hunan Province, China: Constraints from Fluid Inclusions, Trace Elements, and Isotopes. *Ore Geol. Rev.* **2016**, *79*, 1–25.
30. Ding, T.; Ma, D.; Lu, J.; Zhang, R.; Zhang, S.; Gao, S. Petrogenesis of Late Jurassic Granitoids and Relationship to Polymetallic Deposits in Southern China: The Huangshaping Example. *Int. Geol. Rev.* **2016**, *58*, 1646–1672. [CrossRef]

31. Zhu, D.-P.; Li, H.; Algeo, T.J.; Jiang, W.-C.; Wang, C. The Prograde-to-Retrograde Evolution of the Huangshaping Skarn Deposit (Nanling Range, South China). *Miner. Depos.* **2021**, *56*, 1087–1110. [CrossRef]
32. Zhao, L.; Zhang, Y.; Shao, Y.; Li, H.; Ahmad Shah, S.; Zhou, W. Using Garnet Geochemistry Discriminating Different Skarn Mineralization Systems: Perspective from Huangshaping W-Mo-Sn-Cu Polymetallic Deposit, South China. *Ore Geol. Rev.* **2021**, *138*, 104412. [CrossRef]
33. Mao, J.W.; Wu, S.H.; Song, S.W.; Dai, P.; Xie, G.Q.; Su, Q.W.; Liu, P.; Wang, X.G.; Yu, Z.Z.; Chen, X.Y. The World-Class Jiangnan Tungsten Belt: Geological Characteristics, Metallogeny, and Ore Deposit Model. *Sci. Bull.* **2020**, *65*, 3746–3762.
34. Liu, B.; Kong, H.; Wu, Q.-H.; Chen, S.-F.; Li, H.; Xi, X.-S.; Wu, J.-H.; Jiang, H. Origin and Evolution of W Mineralization in the Tongshanling Cu–Polymetallic Ore Field, South China: Constraints from Scheelite Microstructure, Geochemistry, and Nd–O Isotope Evidence. *Ore Geol. Rev.* **2022**, *143*, 104764. [CrossRef]
35. Wu, J.; Kong, H.; Li, H.; Algeo, T.J.; Yonezu, K.; Liu, B.; Wu, Q.; Zhu, D.; Jiang, H. Multiple Metal Sources of Coupled Cu-Sn Deposits: Insights from the Tongshanling Polymetallic Deposit in the Nanling Range, South China. *Ore Geol. Rev.* **2021**, *139*, 104521. [CrossRef]
36. Blevin, P.L. Redox and Compositional Parameters for Interpreting the Granitoid Metallogeny of Eastern Australia: Implications for Gold-rich Ore Systems. *Resour. Geol.* **2004**, *54*, 241–252. [CrossRef]
37. Sun, W.D.; Liang, H.Y.; Ling, M.X.; Zhan, M.Z.; Ding, X.; Zhang, H.; Yang, X.Y.; Li, Y.L.; Ireland, T.R.; Wei, Q.R.; et al. The Link between Reduced Porphyry Copper Deposits and Oxidized Magmas. *Geochim. Cosmochim. Acta* **2013**, *103*, 263–275. [CrossRef]
38. Cheng, Y.; Spandler, C.; Chang, Z.; Clarke, G. Volcanic–Plutonic Connections and Metal Fertility of Highly Evolved Magma Systems: A Case Study from the Herberton Sn–W–Mo Mineral Field, Queensland, Australia. *Earth Planet. Sci. Lett.* **2018**, *486*, 84–93. [CrossRef]
39. Mao, J.; Pirajno, F.; Cook, N. Mesozoic Metallogeny in East China and Corresponding Geodynamic Settings—An Introduction to the Special Issue. *Ore Geol. Rev.* **2011**, *43*, 1–7. [CrossRef]
40. Wu, Q.; Cao, J.; Kong, H.; Shao, Y.; Li, H.; Xi, X.; Deng, X. Petrogenesis and Tectonic Setting of the Early Mesozoic Xitian Granitic Pluton in the Middle Qin-Hang Belt, South China: Constraints from Zircon U–Pb Ages and Bulk-Rock Trace Element and Sr–Nd–Pb Isotopic Compositions. *J. Asian Earth Sci.* **2016**, *128*, 130–148. [CrossRef]
41. Hao, Z.; Xiao, Y.; HuiFu, D.; Wang, Q.; Chang, J.; Shen, L.; Lin, L. Geochemistry of the Cunqian Ore-Bearing Porphyry from the Eastern Qin-Hang Metallogenic Belt and Its Implication for Tectonic Setting and Mineralization. *Acta Petrol. Sin.* **2016**, *32*, 2069–2085.
42. Shi, G.; Xue, J.; Zhu, X.; Pang, Z.; Wang, X.; Yang, F.; Jepson, G.; Tao, W.; Zhen, S. Ore Genesis of the Changkeng–Fuwan Au-Ag Deposit in Central Guangdong, South China: Evidence from Fluid Inclusions and C-H-O-S-Pb-He-Ar Isotopes. *Minerals* **2022**, *12*, 799. [CrossRef]
43. Yu, Z.-F.; Peng, Q.-M.; Zhao, Z.; Wang, P.-A.; Xia, Y.; Wang, Y.-Q.; Wang, H. Geochronology, Geochemistry, and Geodynamic Relationship of the Mafic Dykes and Granites in the Qianlishan Complex, South China. *Minerals* **2020**, *10*, 1069. [CrossRef]
44. Gilder, S.A.; Gill, J.; Coe, R.S.; Zhao, X.; Liu, Z.; Wang, G.; Yuan, K.; Liu, W.; Kuang, G.; Wu, H. Isotopic and Paleomagnetic Constraints on the Mesozoic Tectonic Evolution of South China. *J. Geophys. Res. Solid Earth* **1996**, *101*, 16137–16154. [CrossRef]
45. Quan, T.J.; Wang, G.; Zhong, J.L.; Fei, L.D.; Kong, H.; Liu, S.J.; Zhao, Z.Q.; Guo, B.Y. Petrogenesis of Granodiorites in Tongshanling Deposit of Hunan Province: Constraints from Petrogeochemistry, Zircon U–Pb Chronology and Hf Isotope. *J. Mineral. Petrol.* **2013**, *33*, 43–52.
46. Li, F.S.; Kang, R.H.; Hu, X.Y.; Ma, W.L.; Huang, X.H.; Zeng, Y.H.; Tang, J.B.; Zhu, X.; Qin, Z.W.; Zhao, J. Geological Characteristics and Ore-Search Prospect of the Weijia Tungsten Deposit in Nanling Region. *Geol. China* **2012**, *39*, 445–457.
47. Yang, C.; Shen, Z.J.; Kuang, W.L.; Zhang, W.H. The Geological Features and Minerogenetic Mechanism of Tungsten–Polymetallic Deposits in Tongshanling Area, Southwestern Hunan: Taking Xianglinpu Deposit as an Example. *Contrib. Geol. Miner. Resour. Res.* **2012**, *27*, 156–161.
48. Stacey, J.S.; Kramers, J.D. Approximation of Terrestrial Lead Isotope Evolution by a Two-Stage Model. *Earth Planet. Sci. Lett.* **1975**, *26*, 207–221. [CrossRef]
49. Vermeesch, P. IsoplotR: A Free and Open Toolbox for Geochronology. *Geosci. Front.* **2018**, *9*, 1479–1493. [CrossRef]
50. Balcaen, L.; De Schrijver, I.; Moens, L.; Vanhaecke, F. Determination of the 87Sr/86Sr Isotope Ratio in USGS Silicate Reference Materials by Multi-Collector ICP–Mass Spectrometry. *Int. J. Mass Spectrom.* **2005**, *242*, 251–255. [CrossRef]
51. Jweda, J.; Bolge, L.; Class, C.; Goldstein, S.L. High Precision Sr-Nd-Hf-Pb Isotopic Compositions of USGS Reference Material BCR-2. *Geostand. Geoanal. Res.* **2016**, *40*, 101–115. [CrossRef]
52. Le Maitre, R.W. A Classification of Igneous Rocks and Glossary of Terms. *Recomm. Int. Union Geol. Sci. Subcomm. Syst. Igneous Rocks* **1989**, *193*.
53. Maniar, P.D.; Piccoli, P.M. Tectonic Discrimination of Granitoids. *Geol. Soc. Am. Bull.* **1989**, *101*, 635–643. [CrossRef]
54. Rickwood, P.C. Boundary Lines within Petrologic Diagrams Which Use Oxides of Major and Minor Elements. *Lithos* **1989**, *22*, 247–263. [CrossRef]

55. Sun, S.-S.; McDonough, W.F. Chemical and Isotopic Systematics of Oceanic Basalts: Implications for Mantle Composition and Processes. *Geol. Soc. Lond. Spec. Publ.* **1989**, *42*, 313–345. [CrossRef]
56. Belousova, E.; Griffin, W.; O'Reilly, S.Y.; Fisher, N. Igneous Zircon: Trace Element Composition as an Indicator of Source Rock Type. *Contrib. Mineral. Petrol.* **2002**, *143*, 602–622. [CrossRef]
57. Hoskin, P.W.O.; Schaltegger, U. The Composition of Zircon and Igneous and Metamorphic Petrogenesis. *Rev. Mineral. Geochem.* **2003**, *53*, 27–62. [CrossRef]
58. Wu, Y.; Zheng, Y. Genesis of Zircon and Its Constraints on Interpretation of U-Pb Age. *Chin. Sci. Bull.* **2004**, *49*, 1554–1569. [CrossRef]
59. Huang, X.; Lu, J.; Sizaret, S.; Wang, R.; Ma, D.; Zhang, R.; Zhao, X.; Wu, J. Petrogenetic Differences between the Middle-Late Jurassic Cu-Pb-Zn-Bearing and W-Bearing Granites in the Nanling Range, South China: A Case Study of the Tongshanling and Weijia Deposits in Southern Hunan Province. *Sci. China Earth Sci.* **2017**, *60*, 1220–1236. [CrossRef]
60. Chappell, B.W. Two Contrasting Granite Types. *Pacif. Geol.* **1974**, *8*, 173–174.
61. Loiselle, M.C. Characteristics and Origin of Anorogenic Granites. *Geol. Soc. Am. Abstr. Programs* **1979**, *11*, 468.
62. Miller, C.F. Are Strongly Peraluminous Magmas Derived from Pelitic Sedimentary Sources? *J. Geol.* **1985**, *93*, 673–689. [CrossRef]
63. Whalen, J.B.; Currie, K.L.; Chappell, B.W. A-Type Granites: Geochemical Characteristics, Discrimination and Petrogenesis. *Contrib. Mineral. Petrol.* **1987**, *95*, 407–419. [CrossRef]
64. Chappell, B.W.; White, A.J.R. I-and S-Type Granites in the Lachlan Fold Belt. *Earth Environ. Sci. Trans. R. Soc. Edinb.* **1992**, *83*, 1–26.
65. Chappell, B.W. Aluminium Saturation in I- and S-Type Granites and the Characterization of Fractionated Haplogranites. *Lithos* **1999**, *46*, 535–551. [CrossRef]
66. Davis, J.; Hawkesworth, C. The Petrogenesis of 30–20 Ma Basic and Intermediate Volcanics from the Mogollon-Datil Volcanic Field, New Mexico, USA. *Contrib. Mineral. Petrol.* **1993**, *115*, 165–183. [CrossRef]
67. Xu, H.; Ma, C.; Zhao, J.; Zhang, J. Magma Mixing Generated Triassic I-Type Granites in South China. *J. Geol.* **2014**, *122*, 329–351. [CrossRef]
68. He, H.; Li, Y.; Wang, C.; Han, Z.; Ma, P.; Xiao, S. Petrogenesis and Tectonic Implications of Late Cretaceous Highly Fractionated I-Type Granites from the Qiangtang Block, Central Tibet. *J. Asian Earth Sci.* **2019**, *176*, 337–352. [CrossRef]
69. Quelhas, P.; Mata, J.; Dias, Á.A. Evidence for Mixed Contribution of Mantle and Lower and Upper Crust to the Genesis of Jurassic I-Type Granites from Macao, SE China. *GSA Bull.* **2021**, *133*, 37–56. [CrossRef]
70. Moghadam, H.S.; Li, Q.-L.; Griffin, W.L.; Stern, R.J.; Chiaradia, M.; Karsli, O.; Ghorbani, G.; O'Reilly, S.Y.; Pourmohsen, M. Zircon U-Pb, Geochemical and Isotopic Constraints on the Age and Origin of A-and I-Type Granites and Gabbro-Diorites from NW Iran. *Lithos* **2020**, *374*, 105688. [CrossRef]
71. Clemens, J.D.; Stevens, G.; Farina, F. The Enigmatic Sources of I-Type Granites: The Peritectic Connexion. *Lithos* **2011**, *126*, 174–181. [CrossRef]
72. Chappell, B.W.; Bryant, C.J.; Wyborn, D. Peraluminous I-Type Granites. *Lithos* **2012**, *153*, 142–153. [CrossRef]
73. Topuz, G.; Candan, O.; Zack, T.; Chen, F.; Li, Q.-L. Origin and Significance of Early Miocene High-potassium I-Type Granite Plutonism in the East Anatolian Plateau (the Taşlıçay Intrusion). *Lithos* **2019**, *348*, 105210. [CrossRef]
74. Griffin, W.L.; Wang, X.; Jackson, S.E.; Pearson, N.J.; O'Reilly, S.Y.; Xu, X.; Zhou, X. Zircon Chemistry and Magma Mixing, SE China: In-Situ Analysis of Hf Isotopes, Tonglu and Pingtan Igneous Complexes. *Lithos* **2002**, *61*, 237–269. [CrossRef]
75. Rudnick, R.L.; Gao, S. Composition of the Continental Crust. *Treatise Geochem.* **2003**, *3–9*, 1–64. [CrossRef]
76. Sisson, T.W.; Ratajeski, K.; Hankins, W.B.; Glazner, A.F. Voluminous Granitic Magmas from Common Basaltic Sources. *Contrib. Mineral. Petrol.* **2005**, *148*, 635–661. [CrossRef]
77. Ionov, D.A.; Hofmann, A.W. Nb Ta-Rich Mantle Amphiboles and Micas: Implications for Subduction-Related Metasomatic Trace Element Fractionations. *Earth Planet. Sci. Lett.* **1995**, *131*, 341–356. [CrossRef]
78. Stepanov, A.; Mavrogenes, J.A.; Meffre, S.; Davidson, P. The Key Role of Mica during Igneous Concentration of Tantalum. *Contrib. Mineral. Petrol.* **2014**, *167*, 1009. [CrossRef]
79. Sylvester, P.J. Post-Collisional Strongly Peraluminous Granites. *Lithos* **1998**, *45*, 29–44. [CrossRef]
80. Sun, H.; Li, H.; Danišík, M.; Xia, Q.; Jiang, C.; Wu, P.; Yang, H.; Fan, Q.; Zhu, D. U–Pb and Re–Os Geochronology and Geochemistry of the Donggebi Mo Deposit, Eastern Tianshan, NW China: Insights into Mineralization and Tectonic Setting. *Ore Geol. Rev.* **2017**, *86*, 584–599. [CrossRef]
81. Gao, P.; Zheng, Y.F.; Zhao, Z.F. Experimental Melts from Crustal Rocks: A Lithochemical Constraint on Granite Petrogenesis. *Lithos* **2016**, *266–267*, 133–157. [CrossRef]
82. Yu, J.; Zhou, X.; O'Reilly, Y.S.; Zhao, L.; Griffin, W.L.; Wang, R.; Wang, L.; Chen, X. Formation History and Protolith Characteristics of Granulite Facies Metamorphic Rock in Central Cathaysia Deduced from U-Pb and Lu-Hf Isotopic Studies of Single Zircon Grains. *Chin. Sci. Bull.* **2005**, *50*, 2080–2089. [CrossRef]
83. Yu, J.-H.; O'Reilly, S.Y.; Zhao, L.; Griffin, W.L.; Zhang, M.; Zhou, X.; Jiang, S.-Y.; Wang, L.-J.; Wang, R.-C. Origin and Evolution of Topaz-Bearing Granites from the Nanling Range, South China: A Geochemical and Sr–Nd–Hf Isotopic Study. *Mineral. Petrol.* **2007**, *90*, 271–300. [CrossRef]

84. Eby, G.N. Chemical Subdivision of the A-Type Granitoids:Petrogenetic and Tectonic Implications. *Geology* **1992**, *20*, 641–644. [CrossRef]
85. Altherr, R.; Holl, A.; Hegner, E.; Langer, C.; Kreuzer, H. High-Potassium, Calc-Alkaline I-Type Plutonism in the European Variscides: Northern Vosges (France) and Northern Schwarzwald (Germany). *Lithos* **2000**, *50*, 51–73. [CrossRef]
86. Patiño Douce, A.E. What Do Experiments Tell Us about the Relative Contributions of Crust and Mantle to the Origin of Granitic Magmas? *Geol. Soc. Lond. Spec. Publ.* **1999**, *168*, 55–75. [CrossRef]
87. Jiang, Y.H.; Jiang, S.Y.; Dai, B.Z.; Liao, S.Y.; Zhao, K.D.; Ling, H.F. Middle to Late Jurassic Felsic and Mafic Magmatism in Southern Hunan Province, Southeast China: Implications for a Continental Arc to Rifting. *Lithos* **2009**, *107*, 185–204. [CrossRef]
88. Wang, Y.J. U-Pb Dating of Mesozoic Granodioritic Intrusions in Southeastern Hunan Province and Its Petrogenetic Implication. *Sci. China Ser. D* **2001**, *45*, 271–280.
89. Wei, D.F.; Bao, Z.Y.; Fu, J.M. Geochemical Characteristics and Zircon SHRIMP U-Pb Dating of the Tongshanling Granite in Hunan Province, South China. *Geotecton. Metallog.* **2007**, *31*, 482–489.
90. Barth, M.G.; McDonough, W.F.; Rudnick, R.L. Tracking the Budget of Nb and Ta in the Continental Crust. *Chem. Geol.* **2000**, *165*, 197–213. [CrossRef]
91. Jiang, Y.-H.; Wang, G.-C.; Liu, Z.; Ni, C.-Y.; Qing, L.; Zhang, Q. Repeated Slab Advance–Retreat of the Palaeo-Pacific Plate underneath SE China. *Int. Geol. Rev.* **2015**, *57*, 472–491. [CrossRef]
92. Zhou, X.M.; Li, W.X. Origin of Late Mesozoic Igneous Rocks in Southeastern China: Implications for Lithosphere Subduction and Underplating of Mafic Magmas. *Tectonophysics* **2000**, *326*, 269–287. [CrossRef]
93. Li, Z.-X.; Li, X.-H. Formation of the 1300-Km-Wide Intracontinental Orogen and Postorogenic Magmatic Province in Mesozoic South China: A Flat-Slab Subduction Model. *Geology* **2007**, *35*, 179–182. [CrossRef]
94. Li, X.H.; Li, Z.X.; Li, W.X.; Liu, Y.; Yuan, C.; Wei, G.; Qi, C. U–Pb Zircon, Geochemical and Sr–Nd–Hf Isotopic Constraints on Age and Origin of Jurassic I- and A-Type Granites from Central Guangdong, SE China: A Major Igneous Event in Response to Foundering of a Subducted Flat-Slab? *Lithos* **2007**, *96*, 186–204. [CrossRef]
95. Hu, R.Z.; Chen, W.T.; Xu, D.R.; Zhou, M.F. Reviews and New Metallogenic Models of Mineral Deposits in South China: An Introduction. *J. Asian Earth Sci.* **2017**, *137*, 1–8. [CrossRef]
96. Jiang, S.-Y.; Zhao, K.-D.; Jiang, Y.-H.; Dai, B.-Z. Characteristics and Genesis of Mesozoic A-Type Granites and Associated Mineral Deposits in the Southern Hunan and Northern Guangxi Provinces along the Shi-Hang Belt, South China. *Geol. J. China Univ.* **2008**, *14*, 496.
97. Pirajno, F.; Ernst, R.E.; Borisenko, A.S.; Fedoseev, G.; Naumov, E.A. Intraplate Magmatism in Central Asia and China and Associated Metallogeny. *Ore Geol. Rev.* **2009**, *35*, 114–136. [CrossRef]
98. Fan, C.; Xia, S.; Zhao, F.; Sun, J.; Cao, J.; Xu, H.; Wan, K. New Insights into the Magmatism in the Northern Margin of the S Outh C Hina S Ea: Spatial Features and Volume of Intraplate Seamounts. *Geochem. Geophys. Geosyst.* **2017**, *18*, 2216–2239. [CrossRef]
99. Cao, J.T.; Wang, Y.L.; Wang, J.B.; Zhou, Q.M.; Ma, S.H.; Liu, Y.M. An Electrochemiluminescence Ratiometric Self-Calibrated Biosensor for Carcinoembryonic Antigen Detection. *J. Electroanal. Chem.* **2018**, *814*, 111–117. [CrossRef]
100. Cao, J.; Yang, X.; Du, J.; Wu, Q.; Kong, H.; Li, H.; Wan, Q.; Xi, X.; Gong, Y.; Zhao, H. Formation and Geodynamic Implication of the Early Yanshanian Granites Associated with W–Sn Mineralization in the Nanling Range, South China: An Overview. *Int. Geol. Rev.* **2018**, *60*, 1744–1771. [CrossRef]
101. Roberts, M.P.; Clemens, J.D. Origin of High-Potassium, Calc-Alkaline, I-Type Granitoids. *Geology* **1993**, *21*, 825–828. [CrossRef]
102. Wang, G.C.; Jiang, Y.H.; Liu, Z.; Ni, C.Y.; Qing, L.; Zhang, Q.; Zhu, S.Q. Multiple Origins for the Middle Jurassic to Early Cretaceous High-K Calc-Alkaline I-Type Granites in Northwestern Fujian Province, SE China and Tectonic Implications. *Lithos* **2016**, *246–247*, 197–211. [CrossRef]
103. Harris, R.A.; Stone, D.B.; Turner, D.L. Tectonic Implications of Paleomagnetic and Geochronologic Data from the Yukon-Koyukuk Province, Alaska. *Geol. Soc. Am. Bull.* **1987**, *99*, 362–375. [CrossRef]
104. Pearce, J.A.; Harris, N.B.W.; Tindle, A.G. Trace Element Discrimination Diagrams for the Tectonic Interpretation of Granitic Rocks. *J. Petrol.* **1984**, *25*, 956–983. [CrossRef]
105. Blevin, P.L.; Chappell, B.W. Chemistry, Origin, and Evolution of Mineralized Granites in the Lachlan Fold Belt, Australia; the Metallogeny of I-and S-Type Granites. *Econ. Geol.* **1995**, *90*, 1604–1619. [CrossRef]
106. Blevin, P.L. The Petrographic and Compositional Character of Variably K-Enriched Magmatic Suites Associated with Ordovician Porphyry Cu–Au Mineralisation in the Lachlan Fold Belt, Australia. *Miner. Depos.* **2002**, *37*, 87–99. [CrossRef]
107. Zhang, Y.; Yang, J.-H.; Chen, J.-Y.; Wang, H.; Xiang, Y.-X. Petrogenesis of Jurassic Tungsten-Bearing Granites in the Nanling Range, South China: Evidence from Whole-Rock Geochemistry and Zircon U–Pb and Hf–O Isotopes. *Lithos* **2017**, *278*, 166–180. [CrossRef]
108. Kemp, A.I.S.; Hawkesworth, C.J.; Foster, G.L.; Paterson, B.A.; Woodhead, J.D.; Hergt, J.M.; Gray, C.M.; Whitehouse, M.J. Magmatic and Crustal Differentiation History of Granitic Rocks from Hf-O Isotopes in Zircon. *Science* **2007**, *315*, 980–983. [CrossRef]
109. Williams, I.S.; Ellis, D.J. Pb, U and Th Diffusion in Natural Zircon. *Nature* **1997**, *390*, 159–162.
110. Cherniak, D.J.; Watson, E.B. Pb Diffusion in Zircon. *Chem. Geol.* **2001**, *172*, 5–24. [CrossRef]

111. Watson, E.B.; Harrison, T.M. Zircon Saturation Revisited: Temperature and Composition Effects in a Variety of Crustal Magma Types. *Earth Planet. Sci. Lett.* **1983**, *64*, 295–304. [CrossRef]
112. Ballard, J.R.; Palin, M.J.; Campbell, I.H. Relative Oxidation States of Magmas Inferred from Ce(IV)/Ce(III) in Zircon: Application to Porphyry Copper Deposits of Northern Chile. *Contrib. Mineral. Petrol.* **2002**, *144*, 347–364. [CrossRef]
113. Liu, B.; Wu, Q.H.; Kong, H.; Xi, X.S.; Jiang, J.B.; Li, H.; Cao, J.Y.; Tang, Y.Y. The evolution sequence of granites in the Xitian ore field in Hunan and its tungsten–tin mineralization: Constraints from zircon U–Pb dating and geochemical characteristics. *Earth Sci.* **2022**, *47*, 240–258.
114. Peng, J.T.; Hu, R.Z.; Yuan, S.D.; Bi, X.W.; Shen, N.P. The Time Ranges of Granitoid Emplacement and Related Nonferrous Metallic Mineralization in Southern Hunan. *Geol. Rev.* **2008**, *54*, 617–625.